Earth and Planetary Science Letters 289 (2010) 377–392

Contents lists available at ScienceDirect

Earth and Planetary Science Letters

journal homepage: www.elsevier.com/locate/epsl

Major element chemistry of ocean island basalts — Conditions of mantle melting and heterogeneity of mantle source

Rajdeep Dasgupta [a,*], Matthew G. Jackson [b], Cin-Ty A. Lee [a]

[a] Department of Earth Science, Rice University, 6100 Main Street, MS 126, Houston, Texas 77005, USA
[b] Department of Terrestrial Magnetism, Carnegie Institution of Washington, 5241 Broadbranch Rd., NW, Washington D.C., 20015, USA

ARTICLE INFO

Article history:
Received 31 August 2009
Received in revised form 30 October 2009
Accepted 13 November 2009
Available online 14 December 2009

Editor: L. Stixrude

Keywords:
ocean island basalts
major element chemistry
lithosphere–asthenosphere boundary
mantle heterogeneity
partial melting

ABSTRACT

We estimate average compositions of near-primary, 'reference' ocean island basalts (OIBs) for 120 volcanic centers from 31 major island groups and constrain the depth of lithosphere–asthenosphere boundary (LAB) at the time of volcanism and the possible depth of melt–mantle equilibration based on recently calibrated melt silica activity barometer. The LAB depth versus fractionation corrected OIB compositions (lava compositions, X, corrected to Mg# 73, $X_{OIB}^{\#73}$, i.e., magmas in equilibrium with Fo_{90}, if olivine is present in the mantle source) show an increased major element compositional variability with increasing LAB depths. OIBs erupted on lithospheres <40 km thick approach the compositions (e.g. $SiO_2^{\#73}$, $TiO_2^{\#73}$, $[CaO/Al_2O_3]^{\#73}$) of primitive ridge basalts and are influenced strongly by depth and extent of shallow melting. However, $X_{OIB}^{\#73}$ on thicker lithospheres cannot be explained by melt–mantle equilibration as shallow as LAB. Melt generation from a somewhat deeper (up to 50 km deeper than the LAB) peridotite source can explain the OIB major element chemistry on lithospheres ≤70 km. However, deeper melting of volatile-free, fertile peridotite is not sufficient to explain the end member primary OIBs on ≥70 km thick lithospheres. Comparison between $X_{OIB}^{\#73}$ and experimental partial melts of fertile peridotite indicates that at least two additional melt components need to be derived from OIB source regions. The first component, similar to that identified in HIMU lavas, is characterized by low $SiO_2^{\#73}$, $Al_2O_3^{\#73}$, $[Na_2O/TiO_2]^{\#73}$, and high $FeO^{*\#73}$, $CaO^{\#73}$, $[CaO/Al_2O_3]^{\#73}$. The second component, similar to that found in Hawaiian Koolau lavas, is characterized by high $SiO_2^{\#73}$, moderately high $FeO^{*\#73}$, and low $CaO^{\#73}$ and $Al_2O_3^{\#73}$. These two components are not evenly sampled by all the islands, suggesting a heterogeneous distribution of mantle components that generate them. We suggest that carbonated eclogite and volatile-free, silica-excess eclogite are the two most likely candidates, which in conjunction with fertile mantle peridotite, give rise to the two primitive OIB end members.

1. Introduction

Constraining the compositional heterogeneity of the mantle is of utmost importance to understand ongoing differentiation and dynamics of the Earth. Isotopic and trace elements studies of oceanic basalts and mantle rocks have convincingly demonstrated that the Earth's mantle is heterogeneous in terms of trace elements and long-lived isotopes (e.g. Gast et al., 1964; Hart, 1971; Hofmann and White, 1982; Zindler and Hart, 1986; Weaver, 1991; Hofmann, 1997; Jackson et al., 2007). However, the matter of lithologic or major element heterogeneity in the Earth's mantle in general and in the source regions of oceanic basalts in particular is still debated. The stakes are high because major elements, not trace elements, control the physical properties of the mantle and hence are the geochemical indices most relevant to geodynamicists and seismologists.

There are clues from individual ocean island chains where isotopic variability has been seen to correlate with the major element variability of the erupted basalts. For example, at Hawaii, fractionation corrected shield-stage basalts show positive correlations between $^{143}Nd/^{144}Nd$ and CaO, CaO/Al_2O_3, and FeO* and a negative correlation with SiO_2 (Hauri, 1996). These basalts also show a positive correlation between $^{187}Os/^{188}Os$ and SiO_2 and a negative correlation between $^{187}Os/^{188}Os$ and FeO*. Since the observations by Hauri (1996), similar observation of major element versus isotope correlations have also been made for individual islands of Hawaiian chain (e.g. Mukhopadhyay et al., 2003; Gaffney et al., 2005; Huang and Frey, 2005). Similarly, Kogiso et al. (1997) showed that for Polynesian oceanic basalts, higher $^{206}Pb/^{204}Pb$ is associated with higher CaO, CaO/Al_2O_3, FeO*, and lower SiO_2. Recently it has been demonstrated that also on a global scale long-lived radiogenic isotopes including Sr and Pb are correlated with major and minor elements of oceanic basalts when all the islands in a given ocean island chain are grouped and when individual analyses are plotted (Jackson and Dasgupta, 2008). Jackson and Dasgupta (2008) showed that compositions of shield stage basalts, averaged on ocean island group

* Corresponding author. Tel.: +1 713 348 2664; fax: +1 713 348 5214.
E-mail address: Rajdeep.Dasgupta@rice.edu (R. Dasgupta).

0012-821X/$ – see front matter © 2009 Elsevier B.V. All rights reserved.
doi:10.1016/j.epsl.2009.11.027

basis, yield positive trends in FeO*–$^{206}Pb/^{204}Pb$, CaO/Al_2O_3–$^{206}Pb/^{204}Pb$, K_2O–$^{87}Sr/^{86}Sr$, K_2O/TiO_2–$^{87}Sr/^{86}Sr$, and a negative trend in SiO_2–$^{206}Pb/^{204}Pb$ space.

The strong correlations of major and minor element oxide concentrations and ratios with isotopes suggest that the source regions of oceanic basalts might also be lithologically or mineralogically heterogeneous. However, inferring lithologic variability of the mantle source from the compositions of erupted basalts requires detailed consideration of different condition of melting for a given mantle source (e.g., Klein and Langmuir, 1987; Langmuir et al., 1992). If a plausible range of pressure–temperature conditions and extents of melting of a natural, volatile-free peridotite source [we take natural peridotite xenolith composition, KLB-1, from Kilbourne Hole, New Mexico, USA as our reference, fertile peridotite composition; Takahashi (1986), Herzberg et al. (1990), Hirose and Kushiro (1993), Davis et al. (2009)] fail to reproduce the observed major element variability in OIBs, then only source heterogeneity in terms of major elements and/or volatiles can be unequivocally argued. This requires careful estimation of near-primary basalt compositions from oceanic provinces and comparing them against the possible conditions of melt–mantle equilibration.

Jackson and Dasgupta (2008) compiled a dataset of 659 primitive OIB samples where both Sr–Pb isotopes and major element compositions were previously measured. Estimates for major element compositions of primary melts of a selected group of OIB samples are also given by Herzberg and Asimow (2008) and Herzberg and Gazel (2009). However, attempts to evaluate a global-scale dataset of near-primary magma compositions of individual ocean islands and their relations with plausible conditions of mantle melting have been limited. Jackson and Dasgupta (2008) estimated average major element composition of basalts on an entire ocean island group basis, but owing to the availability of a small number of samples with both isotopes and major element data, average compositional estimates were not constrained for individual islands within an island chain. But the depth of melt generation and melt–mantle equilibration may vary among island chains and within a single hotspot owing to variation in the lithosphere–asthenosphere boundary (LAB), a boundary that is thought to be governed in part by the age of the lithosphere. For example, a deeper LAB is likely to terminate decompression melting at a greater depth whereas a shallower LAB allows decompression melting to continue to a lower pressure. Previous studies have considered the effect of lithospheric thickness control on the chemistry of erupted basalts from the point of view of both major element and trace element data (McBirney and Gass, 1967; Ellam, 1992; Haase, 1996; Humphreys and Niu, 2009). However, no attempt has been made to integrate LAB control, major element chemistry of basalts, experimental constraints on partial melting, and plausible *P*–*T* conditions of melt generations.

In this study, we make use of widely available major element compositions of ocean island basalts and compile a global database of near-primary ocean island basalts for each of 120 individual volcanic islands. We further constrain the plausible conditions of melt–mantle equilibration for each of the individual ocean islands to evaluate whether major element variation in OIBs can result simply from the difference in the conditions of melting of a homogeneous, volatile-free, peridotite source. Based on the comparison between the mean major element compositions of primary basalts, the estimated conditions of their equilibration with the mantle, and laboratory generated partial melt compositions, we demonstrate that the Earth's mantle is heterogeneous in terms of major elements and volatiles. The variation in depth of peridotite melting owing to variation in lithospheric thickness alone, as suggested recently by Humphreys and Niu (2009), cannot produce the major element variability of global OIB array.

2. Approach

To evaluate the global scale major element systematics of ocean island basalts, we analyze the relationships between near-primary natural basalt compositions and the estimated physical conditions of melting. The plausible physical conditions of melting were derived by taking into account the structure of the oceanic plate beneath each island, thermo-barometric constraints, and laboratory experiments on partial melting of mantle lithologies.

2.1. Lithosphere–asthenosphere boundary (LAB) at the time of volcanism

The present-day plate ages for individual volcanic islands were taken based on the recent sea-floor age map of Müller et al. (2008). To estimate the age of the lithospheric plates at the time of volcanism, average eruption ages were subtracted from the present-day sea-floor ages (Fig. 1; Table 1). The average eruption ages for each island were estimated based on available literature data on the minimum and the maximum age of volcanic activities including preshield, shield building, postshield, and rejuvenated stage lavas (Table 1). The depth of LABs at the time of volcanism were estimated based on the plate model of Stein and Stein (1992), with a plate thickness of 106 km and mantle potential temperature of 1315 °C (McKenzie et al., 2005). We recognize that identifying the exact depth of the lithosphere–asthenosphere boundary may be somewhat elusive as the transition is clearly gradational. However, if we define the lithosphere as the mechanical boundary layer and assume that the mechanical boundary layer is controlled by temperature, then we can loosely define the lithosphere–asthenosphere boundary as scaling with a specific temperature isotherm. The exact temperature chosen is not important as we are primarily interested in relative relationships. Table 1 reports the present-day plate ages, the eruption ages of basalts, the age of lithosphere at the time of volcanism, and the estimated LAB depths for individual ocean islands at the time of volcanism. We note, however, that the actual LAB depths beneath ocean islands may depart from depths calculated using the conductive plate cooling model employed here. For example, thermal anomalies and active mantle upwelling beneath ocean islands can perturb the age–thickness correlations predicted by half-space cooling or plate models. Thermal erosion may cause the mechanical boundary layer to thin (e.g., Neugebauer, 1987; Li et al., 2004; Landes et al., 2007) or alternatively, magmatic underplating may cause the lithosphere to thicken (e.g., Watts et al., 1985; Caress et al., 1995; Danobeitia and Canales, 2000; Hall and Kincaid, 2003). Lithospheric thickness beneath hotspots may also remain unmodified with respect to what might be expected for a lithosphere away from any thermal anomaly (Li et al., 2004). Keeping these plausible scenarios in mind, we have also compiled available seismic data for a subset of individual ocean islands that could be interpreted as an estimate of LAB depths beneath ocean islands at the present-day (d_2 in Fig. 1). We compare the eruption age-corrected LAB depths beneath ocean islands (d_1 in Fig. 1) with various key major element compositional parameters that act as proxies for depth of melting. We further compare the d_1 vs $X^{\#73}_{OIB}$ compositions relations with the pressure vs. melt compositions relations for laboratory generated peridotite partial melts under similar conditions.

2.2. Estimating the compositions of average, near-primary, 'reference' ocean island basalts

Major element data of shield, pre-shield, post-shield, and rejuvenated stage lavas from a total of 120 islands for 31 ocean island groups were considered from Indian, Pacific, and Atlantic Ocean basins (GEOROC database :http://georoc.mpch-mainz.gwdg.de/georoc/). In order to capture the global scale variation of major element chemistry of OIBs, we estimated the average compositions of basalts on an island by island basis for each of the 120 islands. We recognize that a given ocean island may have more than one volcanic center but we do not attempt to estimate average basalt compositions on a volcano by volcano basis. Our goal is to test whether a difference

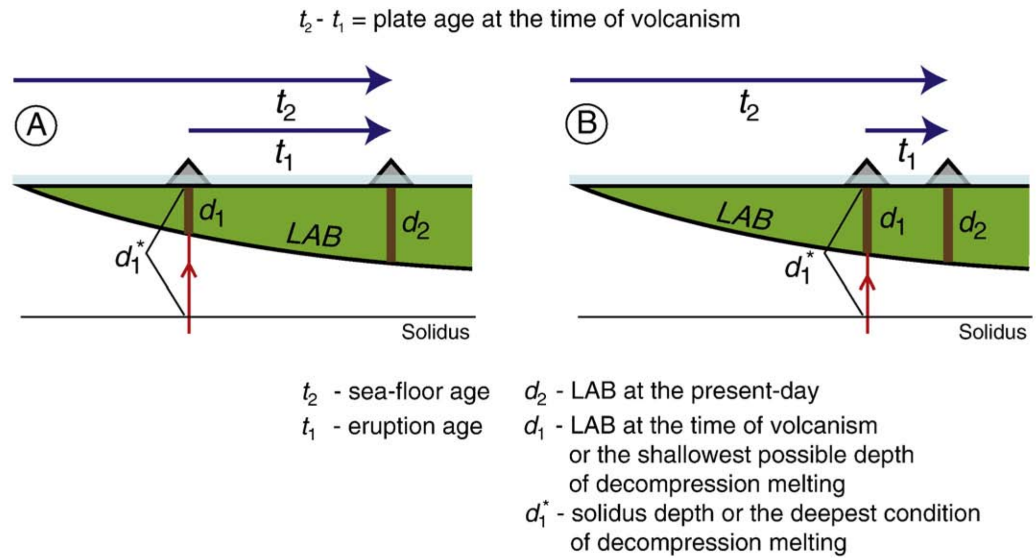

Fig. 1. Cartoon depicting decompression melting beneath ocean islands. Islands situated on younger lithospheres (A) likely sample basalts generated at mean depths that are shallower than islands on older lithospheres (B). To estimate the LAB depths at the time of volcanism (d_1) it is necessary to calculate the mean age of the lithosphere at the time of volcanism, by subtracting eruption ages from the present-day plate ages (t_2–t_1). We note that this correction is small for islands preserving young eruptions (small t_1) on old (t_2 >70 Ma) lithospheres (B) whereas can be significant for islands with old eruption ages (large t_1) on young (t_2 <70 Ma) lithospheres (A). Our estimates of d_1 for 120 oceanic islands based on estimated t_2–t_1 are given in Fig. 2 and Table 1. d_1 gives the shallowest possible depth of decompression melting and the mantle solidus or d_1^* gives the deepest possible depth of decompression melting.

in the physical conditions of decompression melting can explain the variability of OIB major element chemistry globally. Unless the age of volcanoes are very different within an island there will not be any significant difference between their LAB during volcanism or to the depth of the mantle solidus beneath them. This is especially true for islands on old lithospheres where any corrections for eruption ages are small relative to the age of the underlying lithosphere. For example, Hawaii preserves two distinct compositional trends, i.e., Loa and Kea trends, but for our analysis we do not separate these compositions. Similarly, volcanoes that preserve two distinct periods and compositions of eruptive activities, such as Rurutu and Aitutaki in the Cook-Austral chain, are not treated separately. We will show that even after these data smoothing, some of the first order compositional heterogeneity stands out in the global OIB dataset. If we separate out compositional trends or different eruptive episodes within a given island, the argument for heterogeneity will only be stronger.

To minimize the effect of crystal fractionation, especially those of clinopyroxene (cpx) and plagioclase fractionation on the primary OIB chemistry, generally whole-rock or glass samples with 10 wt.%≤MgO≤16 wt.% were considered (Supplementary Table 1). However, a few additional island averages were calculated with MgO as low as 8 wt.%, owing to lack of basalt samples with >10 wt.% MgO (e.g., Azores: Flores and Pico; Easter; Tristan da Cunha: Inaccessible; Galapagos: Genovesa and Santa Fe; Madeira: Unicorn; Mascarene islands: Rodriguez; Pitcairn-Gambier: Fanga Taufa; Samoa: Vailuluu). Intrusive and cumulate rocks were excluded. The concentrations of all the oxides of the selected samples were normalized to 100 wt.%. Comparison of compositions were made both with averages calculated by taking the bin of 10 wt.%≤MgO≤16 wt.% and by correcting the average compositions for crystal fractionation. We observe that even after excluding low MgO (<8 wt.%MgO) lavas, many individual volcanic centers preserve positive MgO–CaO/Al_2O_3 trends, implying component of cpx fractionation (olivine fractionation results in a flat trend in MgO vs. CaO/Al_2O_3 space). We do not make any attempts to determine the exact fractionation path for individual islands, but correct the average compositions to force them to be in equilibrium with olivine of Fo_{90}, i.e., magmas with Mg# of 73. We primarily adopt two different fractionation correction schemes: (1) by adding equilibrium olivine, using Fe^{2+}–Mg K_D of 0.3 (Table 2) and (2) by simultaneously adding olivine and cpx in ratios such that the fractionation path reproduces the slope of MgO–CaO/Al_2O_3 plots for each volcanic centers (Supplementary Table 2). For the latter scheme we use a fixed cpx composition representative of average ocean floor basalts (Nisbet and Pearce, 1977) and for islands with insufficient data to reveal a definite slope in MgO–CaO/Al_2O_3 plot were corrected for olivine fractionation alone (Supplementary Table 2). We have also evaluated the consequence of fractionation of olivine and cpx in fixed proportion (1:4) and using a fixed cpx composition from partial melting experiment on fertile peridotite at 3 GPa (Walter, 1998). We will show, in fact, that the distributions of primitive OIB compositions are not significantly affected by the different fractionation schemes considered here as long as only the high MgO (>8–10 wt.%), near primary basalts are considered. We point out that the fractionation correction schemes considered here may not represent the exact fractionation vector for a given volcanic center. The main uncertainties in estimating the average primary magma compositions are the composition and proportion of fractionating cpx and how they change with progressive crystallization as function of pressure, temperature, and compositions, when cpx is a dominant crystallizing phase, and the Mg# and MgO content of primary magmas. However, our approach does provide necessary fractionation correction so that near-primary, 'reference' compositions from different OIB localities can be compared in light of their source heterogeneities.

3. Observations

3.1. Global-scale correlation between plate thickness and OIB composition

The key features of LAB depth versus X_{OIB} trends are broad positive correlations between LAB depth and maximum magma FeO* and a broad negative correlation between LAB depth and minimum magma SiO_2 for each of Pacific, Atlantic, and Indian Ocean basins globally (Fig. 2 and Supplementary Fig. 1). The correlations are observed by plotting both island averaged lava compositions with 8 wt.%<MgO<16 wt.% (not shown) and by plotting fractionation corrected, island averaged lavas to be in equilibrium with olivine of Fo_{90} (Fig. 2 and Supplementary

Table 1
Present-day plate age, mean eruption age, and LAB depth estimates for ocean islands.

Island groups	Islands	Plate age (Ma)	Eruption age (Ma)	Plate age during volcanism (Ma)	LAB during volcanism (km)	Reference
Atlantic Ocean basin						
Azores	Flores	10	1.1 (11)	8.9 (11)	36.4 −1.8/+1.6	a1
	Faial	13	0.01	13	41.9	a2
	Pico	16	0.03	16	45.3	a3
	Terceira	18	0.185 (185)	17.8 (2)	47.2 −0.2/+0.2	a4
	Sao Miguel	40	0.02	40	67.6	a2, a3, a5
	Santa Maria	47	0.03	47	72.9	a2
Balleny	Sabrina	20	5 (5)	15 (5)	44.2 −6.1/+5.2	a6
	Sturge	24	5 (5)	19 (5)	48.4 −5.3/+4.9	a6
Cameroon	Principe	110	31	79	87.3	a7
	São Tome	106	14	92	90.4	a7
	Bioko/ Fernando Poo	110	15.5 (145)	94.5 (145)	90.9 −3.3/+2.8	a7, a8
	Pagalu	102	5	97	91.4	a7
Canary islands	La Gomera	158	12	146.0	95.9	a9
	La Palma	152	1.77	150.2	96.0	a9
	Tenerife	162	11.6	150.4	96.0	a9
	Gran Canaria	168	14.5	153.5	96.1	a9
	Fuerteventura	178	20.6	157.4	96.2	a9
	Lanzarote	177	15.5	161.5	96.3	a9, a10
	El Hierro	154	1.12	152.9	96.1	a9
Cape Verde	Santo Antaõ	118	3.85 (360)	114.2 (36)	94.4 −0.5/+0.4	a11, a12
	São Vicente	120	3.65 (365)	116.4 (37)	94.7 −0.5/+0.4	a12
	Fogo	124	0.5 (5)	123.5 (5)	95.3	a3
	São Nicolau	127.5	3.1 (3)	124.4 (3)	95.4	a11, a13
	Maio	136	9.25 (275)	126.75 (275)	95.4 −0.1/+0.0	a14
	Santiago	132	3.15 (285)	128.9 (29)	95.5	a12
	Sal	138	8.5 (75)	129.5 (75)	95.5 −0.2/+0.1	a12
	Boa Vista	138	2.5 (25)	135.5 (25)	95.6 −0.1/+0.1	a12
Fernando de Norhona	Fernando de Norhona	95	7.5 (45)	87.5 (45)	89.4 −1.1/+1.0	a15
Gough	Gough	30	0.565 (435)	29.4 (4)	58.4 −0.4/+0.4	a16
Iceland	Iceland	0–20	6.5 (65)	6.5 (30)	32.3 −7.2/+5.0	a17
Jan Mayen	Jan Mayen	0.35	0.35 (35)	0 (4)	0.0 −0.0/+26.6	a18
Madeira	Unicorn seamount	147	27.4	119.6	95.0	a19
	Porto Santo	138	12.7 (16)	125.3 (16)	95.4 −0.1/+0.0	a20
	Seine	152	21.7	130.3	95.4	a19
	Madeira	135	2.65 (195)	132.4 (20)	95.5 −0.1/+0.1	a21
	Chao	138	3.145 (475)	134.9 (5)	95.5	a22
	Deserta Grande	138	3.5 (16)	134.5 (16)	95.5	a22
	Bugio	139	3.12 (119)	135.9 (12)	95.6	a22
Selvagen	Selvagen Pequena	154	29	125	95.4	a23
	Selvagen Grande	154	7.7 (43)	146.3 (43)	95.9 −0.1/+0.1	a23
St Helena	St Helena	40	8 (1)	32 (1)	60.8 −0.9/+0.9	a24
Trindade	Trindade	78	2.5 (25)	75.5 (25)	86.3 −0.8/+0.7	a3, a25
Tristan da Cunha	Inaccessible	20.5	0.3	20.2	49.6	a26
	Tristan da Cunha	22	0.11 (11)	21.9 (1)	51.3 −0.1/+0.1	a26
Indian Ocean basin						
Amsterdam-St. Paul	Amsterdam	0	0 (3)	0	0.0	i1, i2
Comoros	Grande Comore	135	0.065 (65)	134.9 (1)	95.5	i3
	Moheli	137	2.75 (225)	134.3 (23)	95.5 −0.1/+0.1	i3
	Anjouan	137	2.75 (125)	134.3 (13)	95.5	i3
	Mayotte	145	5.65 (250)	139.4 (25)	95.7 −0.1/+0.1	i3
Crozet islands	Ile de l'est	70	4.5 (4.5)	65.5 (85)	82.9 −3.9/+3.0	i4
	Ile de la Possession	71	4.25 (375)	66.75 (75)	83.4 −0.3/+0.3	i5
Heard	Heard	98	22 (22)	76 (22)	86.5 −9.1/+5.1	i6
Kerguelen	Kerguelen	60	27 (3)	33 (3)	61.6 −2.7/+2.6	i6, i7
Mascarene Islands	Rodriguez	13	2.5 (15)	10.5 (15)	38.7 −2.1/+1.9	i8
	Mauritius	61	3.915 (3885)	57.1 (39)	79.0 −2.2/+1.9	i9
	Reunion	67	0.265 (265)	66.7 (3)	83.4 −0.1/+0.1	i10, i11
Prince Edwards islands	Prince Edward	29	0.1075	28.9	57.9	i12
Pacific Ocean basin						
Caroline	Ponape	157	5.8 (28)	151.2 (28)	96.0 −0.1/+0.1	p1
	Kusaie	153	1.9 (7)	151.1 (7)	96.0	p1
	Chuuk	162	8.35 (365)	153.7 (7)	96.1	p1
Cook-Australs	MacDonald seamount	40	13.5 (135)	26.5 (135)	55.7 −13.8/+11.9	p2, p3, p4
	Marotiri	54	4 (2)	50 (2)	74.9 −1.3/+1.3	p2, p3, p4
	Rapa	56	4.25 (125)	51.75 (25)	76.0 −0.2/+0.2	p2, p3, p4
	Raivavae	63	6.5 (10)	56.5 (10)	78.7 −0.5/+0.5	p2, p3, p4
	Tubuai	72	9 (3)	63 (3)	81.9 −1.4/+1.2	p2, p3, p4
	Rurutu	82	10 (4)	72 (4)	85.2 −1.4/+1.2	p2, p3, p4
	Rimatara	86	15 (3)	71 (3)	84.9 −1.0/+1.0	p5
	Mangaia	92	18 (2)	74 (2)	85.9 −0.6/+0.6	p4
	Atiu	96	7.5 (25)	88.5 (25)	89.6 −0.6/+0.6	p4

Table 1 (*continued*)

Island groups	Islands	Plate age (Ma)	Eruption age (Ma)	Plate age during volcanism (Ma)	LAB during volcanism (km)	Reference
Pacific Ocean basin						
	Aitutaki	99	5.5 (35)	93.5 (5)	90.7 −0.1/+0.1	p4
	Rarotonga	96	1.75 (50)	94.25 (50)	90.8 −0.1/+0.1	p4
Easter island	Easter	5	0.6 (3)	4.4 (3)	27.6 −0.8/+0.8	p6
Galapagos	Genovesa	5	2.8	2.2	20.5	p7
	Roca Redonda	5	0.534	4.5	27.8	p8
	Santa Fe	10	2.76	7.24	33.7	p7
	San Cristobal	9.5	1.2 (12)	8.3 (12)	35.5 −2.0/+1.8	a3
	Isabela	11	2.5 (25)	8.5 (25)	35.8 −4.5/+3.6	p9
	Santa Cruz	9	0.348 (237)	8.65 (24)	36.0 −0.4/+0.4	p10
	Santiago	10	0.35 (35)	9.65 (35)	37.5 −0.5/+0.5	p11
	Espanola	14	2.7 (1)	11.3 (1)	39.8 −0.1/+0.1	p7
	Floreana	14	0.80 (72)	13.2 (7)	42.1 −0.8/+0.8	p7, p10
Hawaiian Islands	Oahu	88	3.15 (55)	84.9 (6)	88.8 −0.1/+0.1	p12
	Kauai	90	5.1 (2)	84.9 (2)	88.8	p13
	Molokai	87	1.83 (7)	85.2 (1)	88.8	a3, p14
	Maui	90	1.035 (285)	89.0 (3)	89.7 −0.1/+0.1	p12
	Kahoolawe	90	1.0 (4)	89.0 (4)	89.7 −0.1/+0.1	p14, p15
	Lanai	90	1.28 (4)	88.72 (4)	89.6	a3, p16, p17
	Niihau	94	4.89 (11)	89.11 (11)	89.7	a3
	Loihi	92	0.0535 (535)	91.94 (5)	90.3	p18
	Hawaii	91	0.215 (215)	90.8 (2)	90.1	a3
Juan Fernandez Islands	Robinson Crusoe	30	4.8 (10)	25.2 (1)	54.5 −0.1/+0.1	p19
	Alexander Selkirk	29	1.7 (7)	27.3 (7)	56.4 −0.7/+0.7	p19
Marquesas	Eiao	53	5.8 (5)	47.2 (5)	73.0 −0.3/+0.3	p20
	Hatutu	53	4.9 (1)	48.1 (1)	73.6 −0.1/+0.1	p5
	Fatu Huku	50	1.6 (4)	48.4 (4)	73.8 −0.3/+0.3	p21
	Fatu Hiva	50	1.3	48.7	74.0 −0.0/+0.0	a3, p22
	Hiva Oa	51	2.2 (6)	48.8 (6)	74.1 −0.4/+0.4	p21
	Nuku Hiva	53	4.0 (8)	49 (8)	74.2 −5.8/+4.8	p21
	Tahuata	51.5	2.2 (6)	49.3 (6)	74.4 −0.4/+0.4	a3, p21
	Ua Huka	52	2.30 (94)	49.7 (9)	74.7 −0.6/+0.6	p23
	Ua Pou	53	2.75 (25)	50.25 (25)	75.0 −0.2/+0.2	p21
Pitcairn-Gambier	Bounty	23	0.35 (10)	22.7 (1)	52.1 −0.1/+0.1	p18
	Fangataufa	34	11.25 (165)	22.8 (17)	52.2 −1.7/+1.6	p24
	Gambier	29.5	6.2 (9)	23.3 (9)	52.6 −0.9/+0.9	p24
	Maruroa	36	10.85 (15)	25.2 (2)	54.5 −0.2/+0.2	p24
Samoa	Tau	107	0.5	106.5	93.2	p25
	Ofu	108	0.7	107.3	93.4	p25
	Tutuila	109	1.2	107.8	93.5	p25
	Vailuluu	108	0	108	93.5	p25
	Savaii	113	5.0 (5)	108.0 (5)	93.5 −0.1/+0.1	p25
	Upolu	112	2 (1)	110 (1)	93.8 −0.2/+0.2	p25
	Lalla rookh	120	10	110	93.8	p25
Society islands	Mehetia	66	0.053 (22)	65.95 (2)	83.1	p26
	Tahiti	74	1.0(4)	73.0 (4)	85.6 −0.1/+0.1	p22
	Moorea	75	1.625 (125)	73.4 (1)	85.7	p22
	Huahine	81	2.25 (15)	78.8 (2)	87.2 −0.1/+0.1	p22
	Tahaa	82	2.925 (325)	79.1 (3)	87.3 −0.1/+0.1	p22
	Raiatea	82	2.5 (1)	79.5 (1)	87.4	p22
	Borabora	83	3.3 (2)	79.7 (2)	87.5 −0.1/+0.1	p22
	Maupiti	84	4.25 (35)	79.8 (4)	87.5 −0.1/+0.1	p22

Present-day plate ages are based on sea-floor age estimates of Müller et al. (2008). Values in parentheses for mean eruption ages and plate ages during volcanism are 1σ standard deviation with last significant digits cited and 1.1 (11) should be read as 1.1 ± 1.1 Ma. Ocean island groups are sorted in alphabetical order within each ocean basins and the order of individual islands are based on increasing thickness of LAB during volcanism. Eruption age estimates are based on the following studies - a1. Azevedo and Portugal Ferreira (2006); a2. Feraud et al. (1980); a3. Caplan-Auerbach et al. (2000); a4. Calvert et al. (2006); a5. Moore (1990); a6. Lanyon et al. (1993); a7. Marzoli et al. (2000); a8. Burke (2001); a9. Carracedo et al. (2002); a10. Carracedo et al. (1998); a11. Plesner et al. (2003); a12. Holm et al. (2006); a13. Duprat et al. (2007); a14. Mitchell et al. (1983); a15. Gerlach et al. (1987); a16. Maund et al. (1988); a17. Jancin et al. (1985); a18. Imsland (1986); a19. Geldmacher et al. (2005); a20. Féraud et al. (Féraud et al., 1981); a21. Geldmacher et al. (2000); a22. Schwarz et al. (2005); a23. Geldmacher et al. (2001); a24. Chaffey et al. (1989); a25. Gripp and Gordon (2002); a26. Gass (1967); i1. Johnson et al. (2000); i2. O'Neill et al. (2003); i3. Nougier et al. (1986); i4. Recq et al. (1998); i5. Camps et al. (2001); i6. Weis et al. (2002); i7. Nicolaysen et al. (2000); i8. Naim et al. (2000); i9. Nohda et al. (2005); i10. Gillot and Nativel (1982); i11. Gillot and Nativel (1989); i12. McDougall et al. (2001); p1. Keating et al. (1984); p2. McNutt et al. (1997); p3. Chauvel et al. (1997); p4. Lassiter et al. (2003); p5. Clouard and Bonneville (2004); p6. Haase et al. (1997); p7. White et al. (1993); p8. Standish et al. (1998); p9. O'Connor et al. (2007); p10. Kurz and Geist (1999); p11. Swanson et al. (1974); p12. McDougall (1964); p13. McDougall (1979); p14. Naughton et al. (1980); p15. Sano et al. (2006); p16. Bonhommet et al. (1977); p17. Herrero-Bervera et al. (2000); p18. Guillou et al. (1997); p19. Farley et al. (1993); p20. Dupuy et al. (1987); p21. Desonie et al. (1993); p22. Duncan and McDougall (1976); p23. Clément et al. (2003). P24. Dupuy et al. (1993); p25. Koppers et al. (2008); p26. Binard et al. (1993).

Fig. 1). The correlations do not change appreciably if the lavas are corrected either by fractionation of both cpx and olivine or to equilibrium olivine of higher or lower Fo# in the range 86–92 (not shown). However, the observed global negative correlation in LAB–OIB $SiO_2^{\#73}$ space is observed only when the minimum $SiO_2^{\#73}$ average compositions are considered from the data envelope. When all the individual island averages are considered, from all the ocean basins combined, the $SiO_2^{\#73}$ contents of basalts actually show increasing variation with increasing LAB depths, i.e., average magma $SiO_2^{\#73}$ contents preserve both high and low concentrations for islands situated on thick lithospheres (Fig. 2). A similar 'fan-out' feature is observed for LAB–$FeO^{*\#73}$ space as well, although it is less pronounced compared to

Table 2
Estimates of near-primary, 'reference', average compositions of ocean island basalts (Mg#73; in equilibrium with Fo_{90}).

	n	$SiO_2^{\#73}$	1σ	$TiO_2^{\#73}$	1σ	$Al_2O_3^{\#73}$	1σ	$FeO^{*\#73}$	1σ	$MnO^{\#73}$	1σ	$MgO^{\#73}$	1σ	$CaO^{\#73}$	1σ	$Na_2O^{\#73}$	1σ	$K_2O^{\#73}$	1σ
Atlantic Ocean basin																			
Azores																			
Flores	2	46.30	0.81	1.97	0.18	11.91	0.85	10.71	0.44	0.15	0.03	16.14	1.64	8.97	2.38	2.45	0.80	1.40	0.27
Faial	6	46.17	2.44	2.17	0.31	12.88	1.86	10.13	0.28	0.14	0.01	15.28	3.11	9.45	0.62	2.77	0.55	1.02	0.33
Pico	15	47.01	0.86	2.20	0.22	12.14	1.13	10.11	0.32	0.14	0.01	15.25	1.35	9.51	0.86	2.70	0.49	0.94	0.17
Terceira	5	46.33	0.47	2.01	0.44	11.88	1.14	10.94	0.75	0.16	0.02	16.50	1.28	9.21	1.03	2.19	0.41	0.78	0.11
Sao Miguel	45	45.94	0.80	2.64	0.38	10.44	1.28	10.98	0.76	0.15	0.03	16.55	1.66	10.19	1.26	1.97	0.39	1.14	0.37
Santa Maria	22	45.04	1.36	2.06	0.33	11.84	1.36	11.22	0.81	0.17	0.01	16.92	0.51	9.53	1.36	2.35	0.33	0.87	0.30
Balleny																			
Sabrina	1	44.69	–	2.03	–	11.83	–	12.09	–	0.18	–	18.23	–	6.94	–	2.99	–	1.01	–
Sturge	3	45.72	0.14	2.15	0.02	11.00	0.19	11.08	0.08	0.20	0.02	16.71	0.07	10.08	0.06	2.34	0.16	0.73	0.11
Cameroon																			
Principe	6	42.68	3.41	1.97	1.46	10.22	1.43	12.50	1.42	0.21	0.15	18.83	1.01	10.21	2.07	2.49	0.90	0.89	0.40
São Tome	8	43.06	0.77	3.92	1.00	9.62	0.97	11.91	1.10	0.12	0.04	17.95	0.53	9.32	0.59	2.99	0.60	1.11	0.51
Bioko/Fernando Poo	7	45.90	1.02	2.30	0.51	9.04	1.48	12.24	0.82	0.19	0.16	18.44	1.72	8.84	1.92	1.98	0.48	1.08	0.35
Pagalu	43.12	1.14	2.59	0.30	9.22	1.37	13.07	1.15	0.14	0.05	19.69	2.19	8.87	0.79	2.26	0.43	1.03	0.36	
Canary islands																			
La Gomera	8	44.83	0.75	2.73	0.50	9.29	1.57	11.75	0.60	0.16	0.01	17.69	1.93	11.10	1.16	1.76	0.95	0.69	0.39
La Palma	33	43.11	2.05	2.88	0.86	9.38	1.46	12.71	1.55	0.16	0.03	19.16	1.31	9.71	1.63	2.10	0.56	0.79	0.35
Tenerife	38	43.59	1.66	2.67	0.65	9.54	1.69	12.53	1.28	0.14	0.02	18.88	1.97	10.05	1.64	1.89	0.74	0.72	0.36
Gran Canaria	191	44.29	2.75	3.15	0.52	9.03	1.14	12.43	0.81	0.16	0.02	18.73	1.62	9.03	2.18	2.28	0.54	0.90	0.38
Fuerteventura	69	43.48	1.99	2.44	0.63	10.45	1.14	12.27	0.82	0.14	0.02	18.49	1.16	9.28	1.25	2.40	0.57	1.04	0.35
Lanzarote	123	45.45	2.66	2.05	0.94	12.55	2.94	10.33	2.58	0.14	0.04	15.57	1.55	10.37	1.74	2.61	0.77	0.92	0.40
El Hierro	31	42.05	0.99	2.92	0.51	8.78	1.12	13.56	0.88	0.16	0.03	20.44	1.24	9.08	0.86	2.15	0.43	0.87	0.28
Cape Verde																			
Santo Antaõ	36	41.79	2.05	3.67	0.73	9.24	0.95	12.47	0.60	0.16	0.02	18.80	1.40	10.45	1.30	2.51	0.85	0.91	0.62
São Vicente	28	42.22	2.53	3.12	0.64	10.11	1.16	11.85	0.91	0.16	0.02	17.87	1.64	11.54	1.38	2.20	0.71	0.92	0.35
Fogo	2	41.61	1.99	2.72	0.40	9.79	0.82	12.40	1.49	0.16	0.01	18.69	0.27	10.98	1.22	2.69	0.43	0.95	1.11
São Nicolau	175	42.77	1.68	2.94	0.42	10.57	0.79	11.85	0.48	0.17	0.03	17.86	1.25	10.83	1.05	2.26	0.69	0.76	0.34
Maio	11	40.23	2.39	3.01	0.78	9.66	1.31	11.76	1.14	0.17	0.01	17.72	1.62	13.67	3.45	2.30	0.55	1.48	1.66
Santiago	19	42.95	1.70	2.83	0.48	10.14	1.13	12.09	1.26	0.15	0.02	18.24	1.49	10.79	1.76	1.89	0.81	0.92	0.55
Sal	11	40.35	3.05	2.97	0.31	10.28	1.04	11.68	1.03	0.17	0.01	17.59	1.81	13.10	2.16	2.68	0.80	1.18	0.53
Boa Vista	18	42.63	1.78	3.33	0.60	10.00	0.88	12.34	0.59	0.16	0.02	18.59	1.12	10.25	0.92	1.75	0.26	0.95	0.31
Fernando de Norhona	36	41.41	2.39	2.89	0.77	9.44	1.26	12.64	0.97	0.16	0.05	19.07	1.40	10.44	0.87	2.79	0.66	1.16	0.47
Gough	10	47.12	1.27	2.50	0.20	10.65	1.04	11.27	0.56	0.13	0.01	16.99	1.53	7.40	0.69	2.29	0.47	1.64	0.29
Iceland	301	47.74	0.86	0.84	0.47	13.60	0.92	9.81	1.27	0.16	0.02	14.77	1.31	11.43	1.25	1.54	0.36	0.12	0.24
Jan Mayen	33	47.07	0.76	2.09	0.42	10.59	2.12	10.13	0.98	0.15	0.03	15.26	2.43	11.53	1.31	1.85	0.45	1.34	0.43
Madeira																			
Unicorn seamount	2	39.53	0.54	2.82	0.25	8.41	0.01	13.95	1.44	0.15	0.02	21.03	0.31	11.91	0.56	1.61	0.19	0.60	0.23
Porto Santo	2	46.34	0.61	1.87	0.01	10.16	1.36	10.87	0.14	0.17	0.01	16.41	0.66	12.30	0.71	1.42	0.16	0.46	0.07
Seine	3	42.48	0.25	2.48	0.03	9.73	0.07	12.74	0.09	0.17	0.01	19.20	0.08	9.51	0.03	2.46	0.16	1.23	0.01
Madeira	96	44.21	0.96	2.24	0.27	11.38	0.82	11.76	0.55	0.17	0.04	17.74	1.52	9.45	0.62	2.33	0.54	0.72	0.14
Chao	5	44.97	0.92	2.03	0.40	10.43	1.41	12.35	0.16	0.15	0.01	18.60	1.67	9.15	0.45	1.82	0.38	0.50	0.13
Deserta Grande	12	45.04	0.34	2.11	0.19	10.08	0.79	12.37	0.38	0.15	0.01	18.65	1.21	9.38	0.46	1.68	0.32	0.53	0.09
Bugio	3	45.18	0.46	2.10	0.21	9.90	1.27	12.39	0.26	0.16	0.01	18.68	2.26	9.39	0.49	1.65	0.38	0.55	0.11
Selvagen																			
Selvagen Pequena	1	42.62	–	2.67	–	13.01	–	10.22	–	0.16	–	15.40	–	12.20	–	2.89	–	0.82	–
Selvagen Grande	24	44.31	2.09	2.12	0.22	11.18	0.81	11.27	0.60	0.18	0.02	17.00	1.01	10.07	1.02	2.98	0.42	0.89	0.16
St Helena	18	45.24	0.91	2.24	0.68	10.43	1.35	11.70	1.18	0.15	0.03	17.63	1.81	10.12	0.80	1.81	0.42	0.68	0.18
Trindade	14	40.55	1.82	3.21	0.92	8.49	1.19	13.33	0.85	0.16	0.03	20.11	0.84	9.58	0.89	3.06	1.08	1.51	0.86
Tristan da Cunha																			
Inaccessible	3	46.66	0.66	2.18	0.25	11.36	0.63	10.65	0.18	0.13	0.01	16.07	0.50	8.78	1.66	2.64	0.51	1.53	0.60
Tristan da Cunha	3	41.93	1.27	2.61	0.32	8.35	0.78	14.03	1.06	0.12	0.01	21.15	1.05	9.26	1.20	1.61	0.66	0.94	0.38
Indian Ocean basin																			
Amsterdam-St. Paul																			
Amsterdam	3	48.55	0.35	1.08	0.02	13.91	0.11	8.68	0.15	0.13	0.00	13.16	0.02	12.01	0.10	1.65	0.05	0.40	0.01
Comoros																			
Grande Comore	44	43.93	1.78	1.74	0.20	10.51	0.93	12.07	1.88	0.17	0.02	18.19	1.70	10.07	0.93	2.46	0.52	0.87	0.28
Moheli	25	42.65	2.23	2.43	0.68	8.99	0.75	13.00	0.63	0.17	0.02	19.61	1.22	9.98	0.92	2.39	1.08	0.78	0.43
Anjouan	13	46.25	1.52	1.90	0.32	9.99	1.20	11.79	1.03	0.15	0.02	17.77	1.01	9.46	0.75	2.01	0.51	0.68	0.28
Mayotte	6	43.32	2.58	2.25	0.53	9.58	0.65	12.53	0.45	0.16	0.01	18.90	1.80	9.75	1.07	2.76	0.69	0.76	0.25
Crozet islands																			
Ile de l'est	21	45.68	0.99	2.19	0.20	10.01	0.88	11.57	0.38	0.14	0.01	17.43	1.57	10.24	0.95	1.90	0.22	0.84	0.16
Ile de la Possession	12	45.12	1.80	2.20	0.41	10.05	1.18	11.24	0.85	0.14	0.02	16.95	1.35	12.15	1.50	1.60	0.34	0.54	0.34
Kerguelen-Heard																			
Heard	33	45.85	2.61	3.24	0.82	9.04	1.52	11.75	1.20	0.15	0.06	17.71	2.02	8.49	1.02	2.08	0.37	1.69	0.42
Kerguelen	2	45.94	0.49	1.88	0.28	14.12	1.41	10.91	0.13	0.14	0.03	16.46	0.04	7.69	1.42	2.29	0.14	0.57	0.00
Mascarene Islands																			
Rodriguez	7	47.94	1.01	1.57	0.33	14.33	1.10	9.34	0.61	0.13	0.01	14.07	1.06	8.68	0.60	2.66	0.26	1.27	0.26
Mauritius	56	45.27	0.49	1.49	0.19	11.47	0.53	12.28	0.65	0.14	0.02	18.52	0.66	8.36	0.80	2.09	0.36	0.37	0.33
Reunion	68	46.42	1.08	1.93	0.46	10.98	1.01	11.54	1.25	0.15	0.02	17.39	1.72	9.16	1.52	1.88	0.38	0.54	0.24
Prince Edwards island	4	43.92	0.50	2.59	0.05	8.83	0.22	12.28	0.06	0.16	0.00	18.51	0.62	9.63	0.49	3.29	0.14	0.79	0.27

Table 2 (*continued*)

	n	$SiO_2^{\#73}$	1σ	$TiO_2^{\#73}$	1σ	$Al_2O_3^{\#73}$	1σ	$FeO*^{\#73}$	1σ	$MnO^{\#73}$	1σ	$MgO^{\#73}$	1σ	$CaO^{\#73}$	1σ	$Na_2O^{\#73}$	1σ	$K_2O^{\#73}$	1σ
Pacific Ocean basin																			
Caroline																			
Ponape	7	43.70	3.76	2.70	0.55	9.55	1.37	12.23	0.93	0.16	0.02	18.43	2.11	9.98	1.90	2.35	0.90	0.90	0.48
Kusaie	3	42.84	0.49	2.79	0.25	10.51	1.56	11.69	0.67	0.15	0.00	17.62	0.51	10.90	0.51	2.71	1.67	0.80	0.48
Chuuk	3	43.20	2.11	2.67	0.46	10.13	0.26	11.71	2.44	0.15	0.01	17.64	0.45	10.62	2.84	2.73	0.79	1.16	0.69
Cook-Australs																			
MacDonald seamount	16	44.83	1.74	2.92	0.36	10.74	1.17	11.15	0.63	0.16	0.01	16.79	2.03	10.29	0.65	2.35	0.50	0.77	0.25
Marotiri	2	43.76	2.37	2.71	0.26	9.89	0.86	11.83	0.66	0.16	0.03	17.83	1.65	11.08	1.86	1.97	0.44	0.75	0.22
Rapa	13	44.37	1.23	2.86	0.26	10.62	1.08	12.00	0.50	0.14	0.02	18.09	1.51	8.92	0.78	1.99	0.64	1.00	0.14
Raivavae	11	45.21	0.81	1.92	0.35	10.23	0.19	12.08	0.06	0.15	0.01	18.23	2.29	9.50	1.31	2.09	0.31	0.59	0.04
Tubuai	22	43.71	1.01	2.11	0.44	9.53	1.11	12.73	0.48	0.17	0.01	19.19	2.09	9.82	0.91	2.12	0.72	0.63	0.27
Rurutu	9	44.50	–	2.21	–	9.40	–	12.67	–	0.16	–	19.11	–	9.97	–	1.59	–	0.38	–
Rimatara	1	43.62	0.31	2.39	0.32	8.53	1.01	13.88	3.09	0.13	0.01	20.91	1.54	7.75	1.01	1.54	0.40	1.26	0.12
Mangaia	10	43.72	1.84	2.00	0.37	8.11	1.11	13.33	0.54	0.16	0.02	20.10	2.02	10.53	1.27	1.60	0.62	0.46	0.43
Atiu	6	45.44	1.19	2.12	0.58	9.74	1.22	11.90	3.44	0.18	0.01	17.95	1.36	9.89	0.56	2.03	0.53	0.75	0.24
Aitutaki	35	42.60	0.73	2.06	0.12	9.97	1.20	12.05	0.64	0.17	0.02	18.17	1.09	10.24	0.57	3.45	0.25	1.30	0.14
Rarotonga	5	44.37	2.29	2.70	0.31	9.62	0.70	12.06	0.67	0.17	0.03	18.19	0.63	10.16	1.14	1.78	0.57	0.94	0.42
Easter	13	46.20	2.23	1.73	0.62	13.00	1.11	10.81	0.29	0.14	0.01	16.29	0.26	9.15	2.85	2.32	0.17	0.36	0.24
Galapagos																			
Genovesa	8	47.31	0.26	0.97	0.09	12.58	0.61	10.35	0.48	0.15	0.01	15.62	0.35	10.74	0.44	2.22	0.07	0.05	0.02
Roca Redonda	2	46.08	0.32	2.14	0.06	11.68	0.57	11.64	0.68	0.16	0.01	17.55	0.74	7.49	0.36	2.69	0.07	0.56	0.02
Santa Fe	2	45.93	0.31	1.38	0.34	13.28	0.61	11.07	0.06	0.19	0.08	16.69	0.05	8.97	0.83	2.20	0.52	0.28	0.30
San Cristobal	6	47.05	0.28	1.14	0.25	15.49	0.57	9.15	0.30	0.16	0.01	13.78	0.26	10.74	0.67	2.21	0.22	0.28	0.16
Isabela	105	47.75	0.76	2.49	1.23	12.68	1.72	11.09	1.14	0.15	0.02	16.72	1.27	6.16	2.24	0.76	0.73	2.20	1.18
Santa Cruz	4	46.10	0.61	1.31	0.44	13.88	0.09	10.83	0.31	0.15	0.01	16.32	0.89	8.77	0.77	2.48	0.62	0.16	0.09
Santiago	5	45.96	1.23	1.60	0.35	12.99	0.87	11.02	0.66	0.15	0.02	16.60	1.60	9.28	1.04	2.21	0.47	0.19	0.10
Espanola	2	46.85	0.08	1.38	0.37	14.61	1.53	9.49	0.38	0.16	0.01	14.31	1.44	10.01	0.06	2.44	0.01	0.73	0.47
Floreana	22	46.84	0.67	1.39	0.34	14.06	0.87	9.43	0.87	0.17	0.01	14.22	1.32	10.52	1.75	2.59	0.57	0.78	0.30
Hawaiian Islands																			
Oahu	172	44.05	2.21	1.92	0.27	9.99	1.20	12.57	0.50	0.17	0.01	18.96	1.52	8.91	0.56	2.70	0.60	0.74	0.36
Kauai	138	43.69	1.48	2.14	0.36	9.67	1.00	12.98	0.88	0.16	0.02	19.57	1.83	9.42	1.08	1.82	0.37	0.57	0.20
Molokai	32	46.78	5.26	2.04	0.44	11.36	0.96	11.21	1.60	0.16	0.08	16.89	1.37	9.14	2.11	1.99	1.11	0.42	0.47
Maui	83	45.98	1.75	2.09	0.41	9.90	0.76	12.53	4.00	0.15	0.01	18.88	1.60	8.24	0.63	1.79	0.25	0.43	0.19
Kahoolawe	7	49.04	1.03	1.58	0.21	10.59	0.58	11.57	0.27	0.15	0.01	17.43	1.82	7.72	0.66	1.71	0.38	0.22	0.08
Lanai	9	49.42	3.07	1.59	0.48	10.94	1.15	11.44	1.06	0.15	0.02	17.26	1.45	7.73	1.42	1.35	0.74	0.12	0.34
Niihau	19	45.40	1.55	1.25	0.51	12.71	0.53	11.44	1.15	0.15	0.03	17.25	1.41	9.27	0.22	2.12	0.26	0.40	0.16
Loihi	12	46.48	2.39	1.96	0.35	10.12	0.88	12.13	2.54	0.15	0.03	18.28	1.60	8.77	1.05	1.72	0.55	0.38	0.29
Hawaii	502	48.10	1.05	1.92	0.18	10.46	0.82	11.46	0.51	0.15	0.00	17.26	1.78	8.55	0.57	1.76	0.23	0.35	0.13
Juan Fernandez Islands																			
Robinson Crusoe	16	44.71	1.70	2.36	0.22	10.87	0.85	11.89	0.37	0.17	0.02	17.94	1.75	8.25	0.85	2.83	0.71	0.99	0.43
Alexander Selkirk	4	46.48	0.84	2.01	0.17	10.84	0.75	12.27	0.72	0.14	0.00	18.48	1.82	7.08	1.20	2.16	0.12	0.53	0.63
Marquesas																			
Eiao	7	46.66	2.20	2.47	0.24	10.22	0.90	11.96	0.66	0.15	0.05	18.04	0.82	8.01	1.01	1.88	0.33	0.61	0.28
Hatutu	9	46.58	0.96	2.55	0.44	9.81	1.41	11.45	0.86	0.17	0.01	17.26	2.18	9.37	0.83	1.87	0.52	0.93	0.36
Fatu Huku	7	46.87	0.62	2.64	0.30	8.94	1.33	12.00	0.56	0.17	0.01	18.09	2.57	8.32	0.93	1.89	0.39	1.07	0.14
Fatu Hiva	12	45.49	0.56	2.66	0.16	10.59	0.21	11.90	0.26	0.16	0.00	17.95	0.35	8.47	0.67	1.88	0.05	0.90	0.14
Hiva Oa	12	45.26	1.34	2.86	0.42	9.77	1.17	12.44	0.67	0.15	0.03	18.74	1.77	7.86	0.83	1.96	0.31	0.96	0.28
Nuku Hiva	12	45.49	1.70	2.45	0.60	9.96	0.78	12.50	0.86	0.14	0.01	18.84	0.92	7.98	0.95	1.90	0.86	0.76	0.25
Tahuata	4	46.24	0.98	2.65	0.74	9.63	0.88	12.02	0.59	0.17	0.01	18.11	1.06	8.51	1.47	1.78	0.43	0.89	0.50
Ua Huka	5	44.46	2.08	2.53	0.24	10.18	1.22	12.16	0.52	0.15	0.02	18.32	3.35	9.25	1.10	2.32	0.30	0.63	0.20
Ua Pou	7	44.47	1.74	2.73	0.63	10.11	0.92	12.30	0.53	0.15	0.03	18.54	2.55	8.46	1.26	2.42	0.41	0.83	0.46
Pitcairn-Gambier																			
Bounty	4	47.55	1.01	2.21	0.11	11.56	0.60	11.12	0.36	0.14	0.01	16.75	0.82	6.95	0.15	2.74	0.20	0.99	0.27
Fangataufa	2	46.22	1.12	2.04	0.13	11.62	0.66	11.29	0.36	0.13	0.00	17.03	0.47	9.06	1.20	2.07	0.49	0.56	0.54
Gambier	2	48.14	1.62	1.85	0.18	11.37	0.69	10.78	0.25	0.15	0.01	16.25	1.17	9.27	0.18	1.69	0.10	0.48	0.08
Maruroa	3	44.72	1.20	2.38	0.86	10.20	0.48	13.02	0.41	0.14	0.01	19.62	0.64	2.96	5.33	1.16	0.78	5.79	5.09
Samoa																			
Tau	18	45.58	1.00	2.74	0.27	9.45	0.92	12.21	0.56	0.15	0.01	18.43	2.05	8.86	0.85	1.89	0.28	0.69	0.12
Ofu	1	43.35	–	3.23	–	8.37	–	13.64	–	0.14	–	20.54	–	8.37	–	1.59	–	0.77	–
Tutuila	10	44.70	2.33	2.97	0.96	9.75	1.07	12.40	0.72	0.15	0.02	18.69	1.61	8.15	0.61	2.17	0.73	1.02	0.42
Vailuluu	13	46.43	0.94	2.19	0.26	10.39	0.83	11.07	0.69	0.14	0.02	16.71	1.37	10.50	0.70	1.88	0.26	0.69	0.09
Savaii	34	45.55		2.66		10.71		11.56		0.14		17.43		8.33		2.38		1.23	
Upolu	29	43.71	1.21	3.18	0.30	9.44	0.98	12.85	0.64	0.13	0.01	19.39	1.72	8.00	0.77	2.24	0.46	1.07	0.45
Lalla rookh	6	41.82	1.77	3.17	0.36	8.48	1.08	13.20	0.53	0.15	0.01	19.90	1.88	9.61	1.56	2.20	0.42	1.47	0.78
Society islands																			
Mehetia	17	43.78	0.83	2.89	0.32	9.23	0.69	12.71	0.37	0.15	0.01	19.15	1.53	8.62	0.41	2.33	0.42	1.14	0.44
Tahiti	44	44.74	1.80	2.57	0.40	9.32	1.76	12.11	1.82	0.15	0.03	18.27	1.45	9.98	2.78	1.91	0.58	0.95	0.40
Moorea	1	46.61	0.77	2.71	0.09	10.33	0.35	11.60	0.39	0.14	0.01	17.49	1.09	8.34	0.42	1.73	0.17	1.05	0.40
Huahine	16	46.74	0.40	2.31	0.16	10.28	1.57	11.54	0.40	0.15	0.00	17.39	0.42	8.31	0.58	1.97	0.20	1.32	0.56
Tahaa	9	47.28	1.70	2.62	0.27	10.38	0.68	11.37	0.40	0.13	0.01	17.12	0.80	7.81	1.13	1.84	0.64	1.46	0.37
Raiatea	3	43.34		3.12		9.10		12.95		0.14		19.54		8.72		2.08		1.00	
Borabora	5	46.97	0.56	2.35	0.47	9.93	1.36	11.49	0.61	0.14	0.01	17.34	2.43	8.70	0.79	2.01	0.14	1.07	0.44
Maupiti	3	47.88	0.55	2.19	0.41	9.56	1.38	11.67	0.09	0.14	0.00	17.58	0.76	7.81	0.37	2.13	0.27	1.05	0.01

The average, 'reference' compositions for each islands are based on glass or whole–rock compositions with 8–16 wt.% MgO (most islands with 10–16 wt.% MgO) and are given in Supplementary Table 1. All the average compositions reported in this table are corrected for olivine fractionation, by adding back equilibrium olivine, using Fe^{2+}–Mg KD of 0.3. The resulting magma compositions (Mg# 73) are all in equilibrium with Fo_{90}. *n* denotes number of samples averaged. 1σ uncertainties are based on the original basalts compositions.

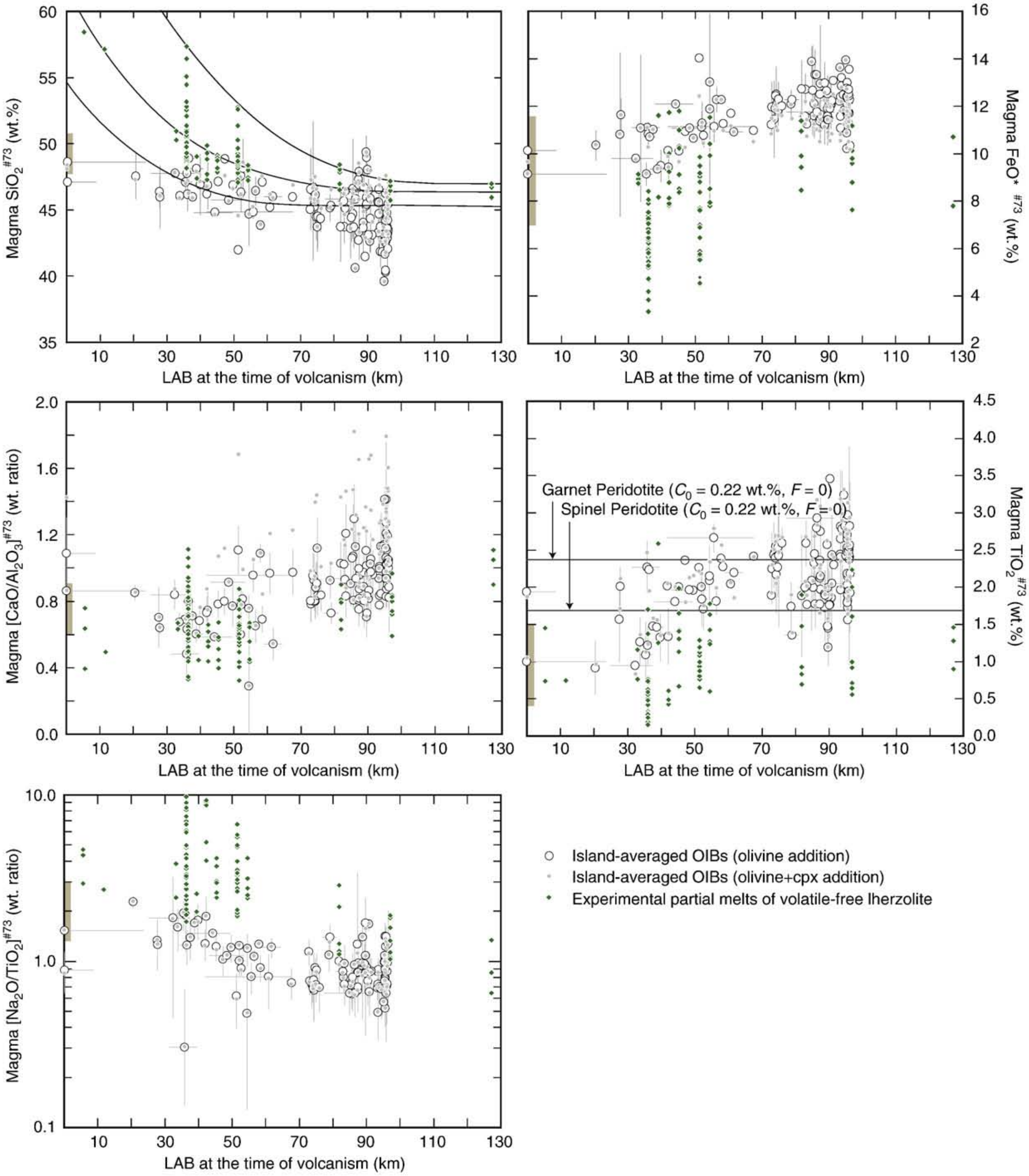

Fig. 2. Island averaged, primitive basalts compositions as a function of depths of LAB at the time of volcanism, d_1. All the island-averaged OIB compositions are fractionation corrected to Mg#73, either by adding equilibrium olivine only (open circles; Table 2) or by adding olivine and cpx in different proportions to match the MgO–CaO/Al_2O_3 trend of each islands (grey circles; Supplementary Table 2). Also plotted for comparison are volatile-free peridotite-derived experimental partial melts from a range of *P–T* conditions and fractionation corrected MORB data (grey vertical bars along *y*-axes) from PetDB database. The lines in depth-SiO_2 space represent 4th order polynomial fit for average, minimum, and maximum limits of SiO_2 contents of experimental partial melts of volatile-free peridotite as a function of depth. Depth-TiO_2 plot also shows the maximum limits of TiO_2 enrichment (melt fraction, $F=0$) in lavas if primary magmas derive from a primitive, fertile peridotite source (0.22 wt.% TiO_2; Prytulak and Elliot, 2007). Any finite extent of melting or derivation from a more depleted source will lower these maximum limits. The error bars for olivine added compositions are 1σ standard deviation of island averaged basalts. The compositional error bars for olivine ± cpx corrected data are not included for clarity.

LAB–$SiO_2^{\#73}$ trend. Minor element oxide concentrations (e.g., $TiO_2^{\#73}$) and ratios (e.g., $[Na_2O/TiO_2]^{\#73}$), and major element oxide ratios such as $[CaO/Al_2O_3]^{\#73}$ also show an overall increase with lithospheric thickness (Fig. 2), but again we note that the spread in the island averaged $TiO_2^{\#73}$, $[CaO/Al_2O_3]^{\#73}$, and $[Na_2O/TiO_2]^{\#73}$ remains significant, especially for islands on a thicker lithosphere.

The dataset of seismic estimates of lithospheric thicknesses beneath ocean islands is limited. However, the dataset comprising the islands of Hawaii, Iceland, Cape Verde, Jan Mayen, and Galapagos, also suggest similar LAB vs. magma SiO_2 and FeO* correlations described above (Fig. 3). This likely suggests that the LAB depth–composition correlations observed in the global OIB dataset are not greatly affected by LAB depth modifications, if any, beneath intraplate ocean islands.

3.2. Regional-scale correlation between plate thickness and OIB composition

Control of lithospheric thickness on chemistry of oceanic basalts has previously been pointed out for a number of individual ocean island

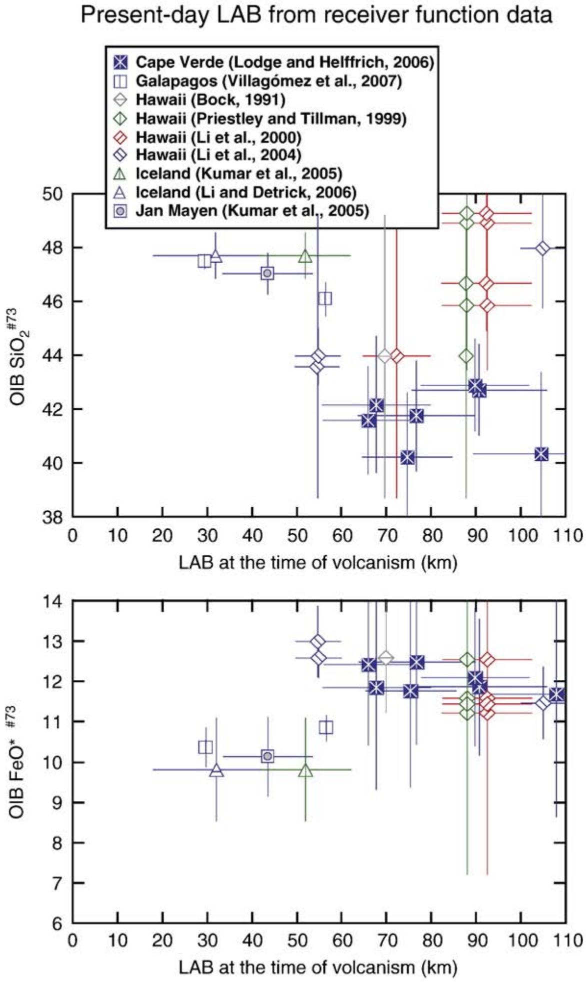

Fig. 3. Island averaged $SiO_2^{\#73}$ and $FeO^{*\#73}$ (fractionation corrected by adding equilibrium olivine; Table 2) of OIBs as a function of LAB depths at the time of volcanism, where the present-day LABs (d_2 in Fig. 1) are estimates based on seismic receiver function studies (Bock, 1991; Priestley and Tilmann, 1999; Li et al., 2000; Li et al., 2004; Kumar et al., 2005; Lodge and Helffrich, 2006; Li and Detrick, 2006; Villagómez et al., 2007). Error bars in compositions are 1σ of the mean and those for LAB depths derive from uncertainties in receiver function estimates and average eruption ages.

groups (e.g., Prytulak and Elliot, 2007; Elliott et al., 2007). The present study also allows us to evaluate the regional-scale correlation between LAB and major element composition of OIBs. We find that the correlations between OIB $SiO_2^{\#73}$, $FeO^{*\#73}$ and LAB depths are less clear for most of the individual ocean island groups, primarily owing to a small variation of LAB depths from island to island within a given ocean island group. However, the island groups that span a LAB depth range at the time of volcanism of ≥30 km do show LAB-$SiO_2^{\#73}$ and LAB- $FeO^{*\#73}$ trends that mimic the global trends. The island groups to be noted in this regard are Azores, Cook-Australs, Mascarene, and Kerguelen-Heard. On the contrary, the islands of Galapagos do not preserve any clear trend. On the other hand, if the prediction of LAB by seismic receiver function study of Li et al. (2004) is accurate, then Hawaii is the only exception to the global trend, as LAB depths correlate positively and negatively with $SiO_2^{\#73}$ and $FeO^{*\#73}$ respectively.

4. Discussion

4.1. The role of LAB in controlling OIB major element chemistry?

A broad negative correlation between the lower bound of the island-averaged magma $SiO_2^{\#73}$ and LAB and a positive correlation between island averaged $FeO^{*\#73}$ and LAB indicate that lithospheric thickness likely provides some control on the mean compositions of basalts for a subset of ocean islands, with deeper LAB causing generation of deeper melts with lower $SiO_2^{\#73}$ and higher $FeO^{*\#73}$. Similarly, broadly increasing $TiO_2^{\#73}$ and $[CaO/Al_2O_3]^{\#73}$, and decreasing $[Na_2O/TiO_2]^{\#73}$ with increasingly deeper LAB indicates overall deeper melt–mantle equilibration for islands on thicker lithospheres. However, if LAB depth provides the sole control on depth of melting of a homogeneous peridotitic mantle then we should expect (1) a steady decrease of $SiO_2^{\#73}$ and an increase of $FeO^{*\#73}$, $[CaO/Al_2O_3]^{\#73}$, and $TiO_2^{\#73}$, with depth and (2) the near-primary magma compositions to match closely with the experimental partial melt compositions at a pressure of interest, i.e., at or near the pressures of LAB. Instead, we observe an increased variability in compositions (e.g., $SiO_2^{\#73}$, $FeO^{*\#73}$, $TiO_2^{\#73}$) with LAB depth. As we will show, the experimental partial melt compositions of peridotites also show a poor fit to the near-primary OIB melt compositions, if melt–mantle equilibration only at LAB depth is considered.

In Fig. 2 we also compare the compositional proxies of OIBs that are sensitive to the pressure of melting with the experimental partial melts of volatile-free peridotite from a range of pressures. It can be noted in Fig. 2 that for an island on intermediate to thin lithospheres, $SiO_2^{\#73}$ and $FeO^{*\#73}$ tend to be lower and higher respectively as compared to what can be generated by partial melting of volatile-free peridotite at that pressure. We note that this conclusion does not change whether fractionation correction for OIBs is made by olivine addition or olivine + cpx addition. The discrepancy between OIB $SiO_2^{\#73}$ and peridotite partial melts also does not change if the LAB depths are calculated based on half-space cooling model (not shown) rather than plate model. This may suggest that the equilibration between average OIBs and the mantle occurs deeper than the LABs, owing to the melting column extending to some distance beneath the LAB. In the next section we evaluate whether melt–mantle equilibration deeper than LAB is sufficient to explain the entire spectrum of OIB major element chemistry, especially for islands on lithospheres of >70–80 Myrs or older.

4.2. Can melt–mantle equilibration deeper than LAB explain the full range of OIB chemistry on thick lithospheres?

The mismatch between peridotite partial melts and primary OIBs at estimated LAB depths lead us to explore the possibility that perhaps melt–mantle equilibration deeper than the LAB can explain all the OIB major element features globally. In order to constrain the depth of mean OIB extraction, we used the recently calibrated melt silica activity barometer of Lee et al. (2009). We assume that all the OIBs equilibrated with a mantle containing olivine and opx and average olivine composition of the mantle is Fo_{90}. Fig. 4 shows the estimates of average depth of equilibration for island averaged, fractionation corrected OIBs versus the estimates of LAB depths. We find that with the exception of Hawaii (and perhaps one island each from the Comoros, Samoa and Canaries), average compositions of all the other ocean islands produce depths of equilibration that are deeper than LAB by ~0–70 km. We point out that discrepancies between LAB depths (predicted by plate model or receiver function studies) and melt–mantle equilibration depths of the order of 0–30 km are perhaps not significant given the uncertainties in estimating LABs and in estimating mean depth of melt–mantle equilibration. We also note that derivation of Hawaiian tholeiites from an olivine-bearing source was recently questioned (Sobolev et al., 2005, 2007), and hence application of melt silica-activity barometer may be problematic for many of the Hawaiian island basalts. However, there still remain a number of ocean islands where conditions of melt–mantle equilibration, as predicted by barometry, are systematically deeper than LAB (Fig. 4). This led us to test whether depths of volatile-free peridotite melt generation that are as much as 70 km deeper than LAB can produce all the aspects of OIB major element chemistry.

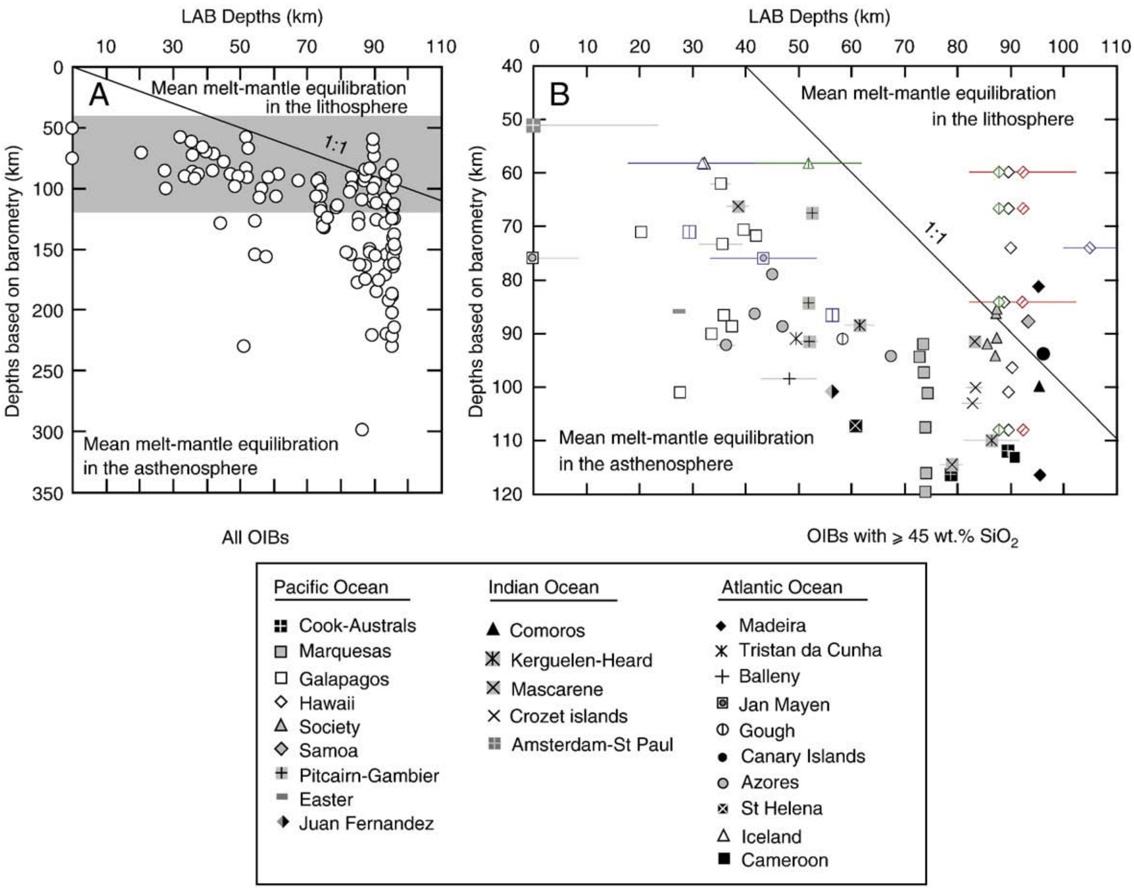

Fig. 4. Estimates of LAB depths versus average depths of equilibration for island averaged, primary OIB compositions (A: Island-averaged OIBs from all the ocean islands compiled in our study; B: Island-averaged OIBs with ≥45 wt.% SiO_2). The mean depth of melt–mantle equilibration is based on melt silica activity barometer of Lee et al. (2009), which assumes that the melt derives from an olivine + opx bearing source. We note that melt–mantle equilibration depths for many ocean islands in panel (A) are likely overestimates as the barometer (Lee et al., 2009) is not particularly calibrated for silica-undersaturated mantle melts. The data points plotting above the 1:1 line suggests apparent depth of equilibration in the oceanic lithosphere whereas islands plotting below the line reflect average melt–mantle equilibration deeper than LAB. The plots suggest that most of the primary OIBs (even when only the OIBs with ≥45 wt.% SiO_2 are considered) globally derive from depths greater than LAB. The only apparent exception is Hawaii, where many of its islands seem to have 'average' melt–mantle equilibration shallower than LAB. The data symbols are same as in Fig. 3 and Supplementary Fig. 1. The shaded region in (A) represents the space in (B).

Comparison of OIB $SiO_2^{\#73}$ with the peridotite partial melts of variable pressures indeed indicate that basalts erupted on thin to intermediate thickness lithospheres (LAB at the time of volcanism of ≤70 km) can be reproduced if the mean depth of melt–mantle equilibration is 20–40 km deeper than LAB. The deviation between OIB $SiO_2^{\#73}$ and SiO_2 of experimental partial melts of peridotite, or

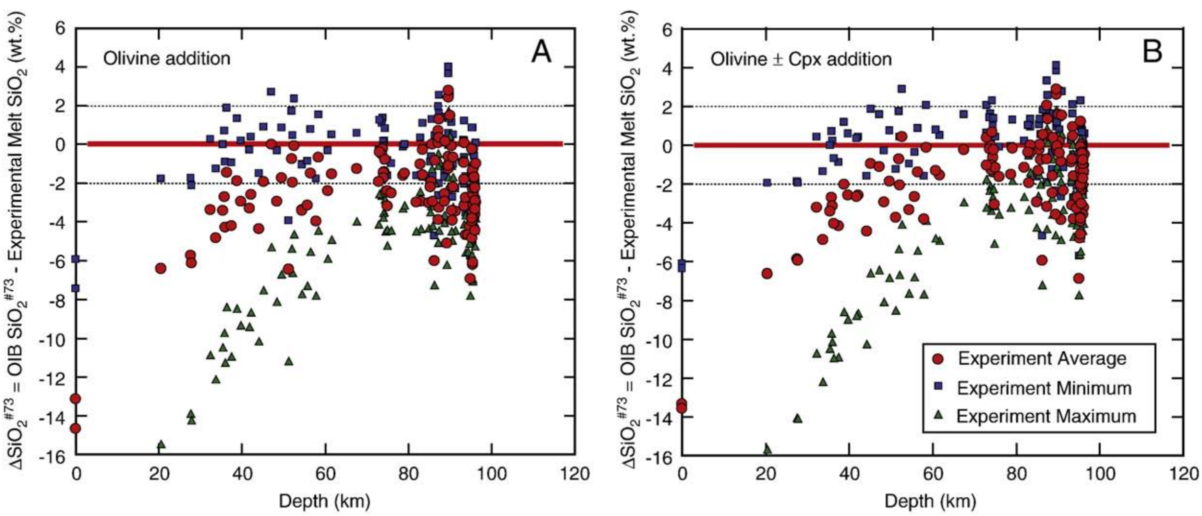

Fig. 5. The difference between fractionation corrected (A: olivine addition; Table 2 and B: olivine + cpx addition; Supplementary Table 2) primary OIB SiO_2 and SiO_2 content of experimental partial melts, $\Delta SiO_2^{\#73}$ as a function of depth, where $\Delta SiO_2^{\#73}$ are measured at estimated LAB depths at the time of volcanism. The approach of $\Delta SiO_2^{\#73}$ from negative values to zero for LAB variation from zero to 70 km may indicate that the average depth of equilibration occurs somewhat deeper than LAB at the time of volcanism. However, the positive and negative excursions of $\Delta SiO_2^{\#73}$ for LAB >70 km cannot be eliminated even by deeper melting of volatile-free, mantle peridotite.

$\Delta SiO_2^{\#73}$ (wt.%), increases steadily from ≤−6 wt.% at LAB of 0 to ~0 wt.% at LAB of 20–70 km depth (Fig. 5). This suggests that if the average depth of equilibration is 20–70 km deeper than LAB then there is no significant difference between volatile-free peridotite partial melts and primitive OIBs. However, basaltic eruptions on thick oceanic lithospheres, i.e., LAB at the time of volcanism of ≥70 km, preserves both positive and negative $\Delta SiO_2^{\#73}$ (Fig. 5). Firstly, if OIBs are partial melts from a homogeneous peridotite source similar to that of KLB-1 (Takahashi, 1986; Herzberg et al., 1990; Davis et al., 2009) (in the presence of olivine and opx), LAB depth versus $\Delta SiO_2^{\#73}$ relations should preserve only negative or near-zero $\Delta SiO_2^{\#73}$ values and not also positive values as high as +4 wt.% as observed in Fig. 5. More importantly, the negative values of $\Delta SiO_2^{\#73}$ of the order of −4 to −8 wt.% remain for islands on thick lithospheres and these differences are too large to be explained by melt generation at conditions that are deeper than LAB even by >50–100 km. This suggests that

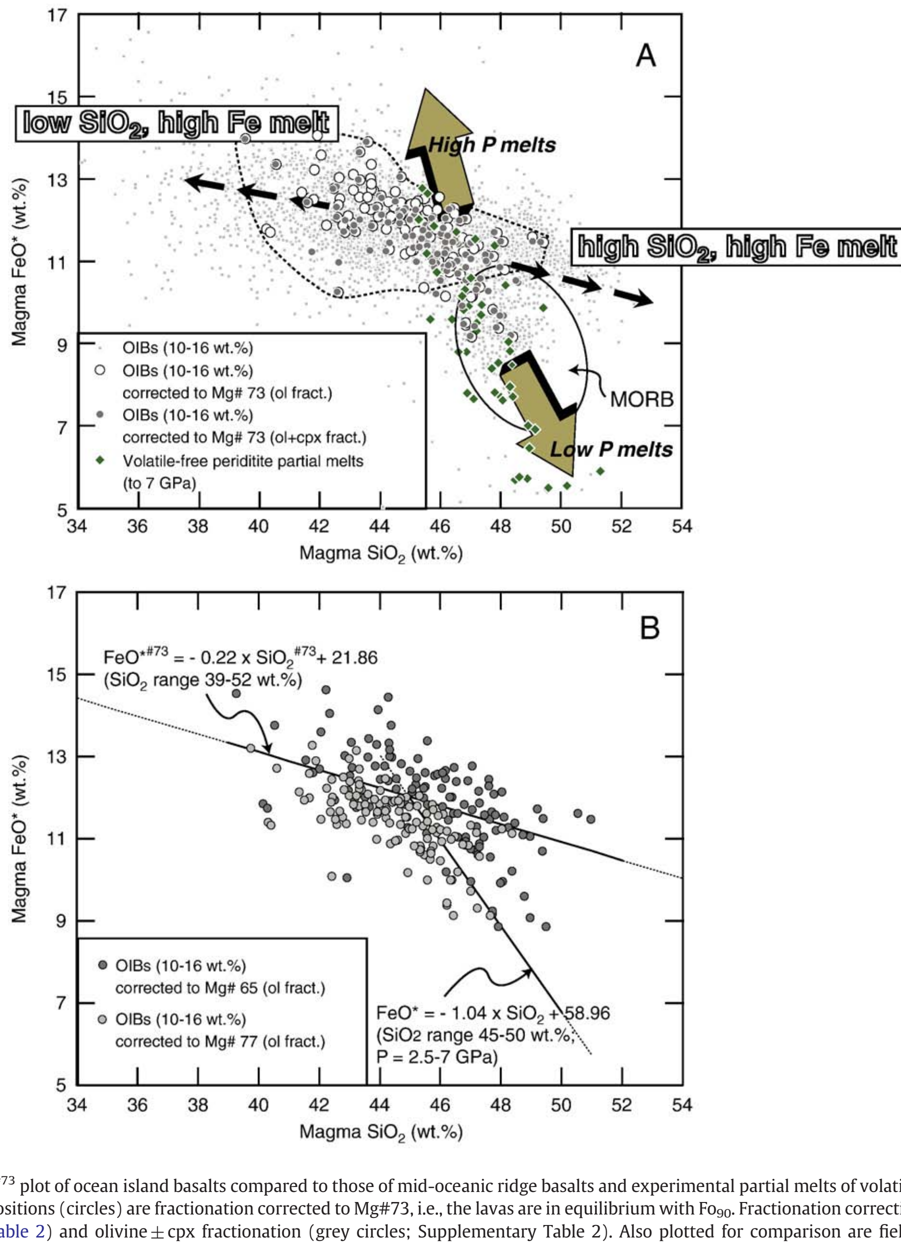

Fig. 6. (A) $FeO^{*\#73}$ versus $SiO_2^{\#73}$ plot of ocean island basalts compared to those of mid-oceanic ridge basalts and experimental partial melts of volatile-free peridotite. All the island-averaged oceanic basalt compositions (circles) are fractionation corrected to Mg#73, i.e., the lavas are in equilibrium with Fo_{90}. Fractionation correction schemes include both olivine fractionation (open circles; Table 2) and olivine ± cpx fractionation (grey circles; Supplementary Table 2). Also plotted for comparison are field of fractionation corrected (in equilibrium with Fo_{90}) MORB from PetDB database, original OIB compositions with MgO between 10 and 16 wt.% (small grey squares), and partial melt compositions generated in laboratory experiments from nominally volatile-free peridotite (green diamonds). Experimental partial melts to pressures up to 7 GPa are from the following studies: Takahashi (1986), Grove and Juster (1989), Kinzler and Grove (1992), Hirose and Kushiro (1993), Baker et al. (1995), Kushiro (1996), Kinzler (1997), Walter (1998), Robinson et al. (1998), Falloon et al. (1999), Pickering-Witter and Johnston (2000), Falloon et al. (2001), Schwab and Johnston (2001), Bulatov et al. (2002), Wasylenki et al. (2003), Laporte et al. (2004), Villiger et al. (2004), and Davis et al. (2009). Only the experiments with three (olivine + opx + cpx/gt/spinel/plagioclase) or four-phase lherzolite (olivine + opx + cpx + gt/spinel/plagioclase) are plotted. The dotted line marks the field of olivine fractionation corrected OIBs with the ridge-influenced islands (Galapagos, Azores, Iceland, Amsterdam-Saint Paul, Easter) excluded. The slope of the Fe–Si trend in primary OIBs is gentler compared to the slope of peridotite partial melts and MORB and the difference in pressure of melting of peridotite (indicated by thick brown arrows) cannot reproduce the trend of intraplate magmas. The extrema of the OIB trend, one with low SiO_2 and high FeO* and the other with high SiO_2 and moderately high FeO*, are not produced by volatile-free peridotite partial melting and thus require at least two additional components in the OIB mantle source region. (B) The effect of fractionation correction on Fe–Si trend of island-averaged OIBs. The average compositions are corrected to Mg# 65 (dark grey circles; equilibrium olivine added until the lavas are in equilibrium with Fo_{86}) and Mg# 77 (light grey circles; equilibrium olivine added until the lavas are in equilibrium with Fo_{92}). Also plotted for comparison, are the best fit lines of $Fe^{\#73}$–$Si^{\#73}$ data of intraplate OIBs (on or near-ridge islands excluded, i.e., a fit based on the open circles within the stippled region in (A)) and volatile-free peridotite partial melts trend based on 2.5–7 GPa data. It can be noted that the slope of the OIB Fe–Si trend is not changed by correcting lavas to a different Mg# and the volatile-free peridotite partial melts trend is always oblique to the natural, intraplate ocean island basalts.

even deeper melting of volatile-free peridotite cannot explain the higher and lower end of the distribution of OIB $SiO_2^{\#73}$ and additional melt components are required to be generated from the OIB source mantle.

4.3. FeO*–SiO_2 correlations in primary OIBs

Perhaps the most convincing argument for the major element heterogeneity of the OIB source mantle comes from the analysis of the

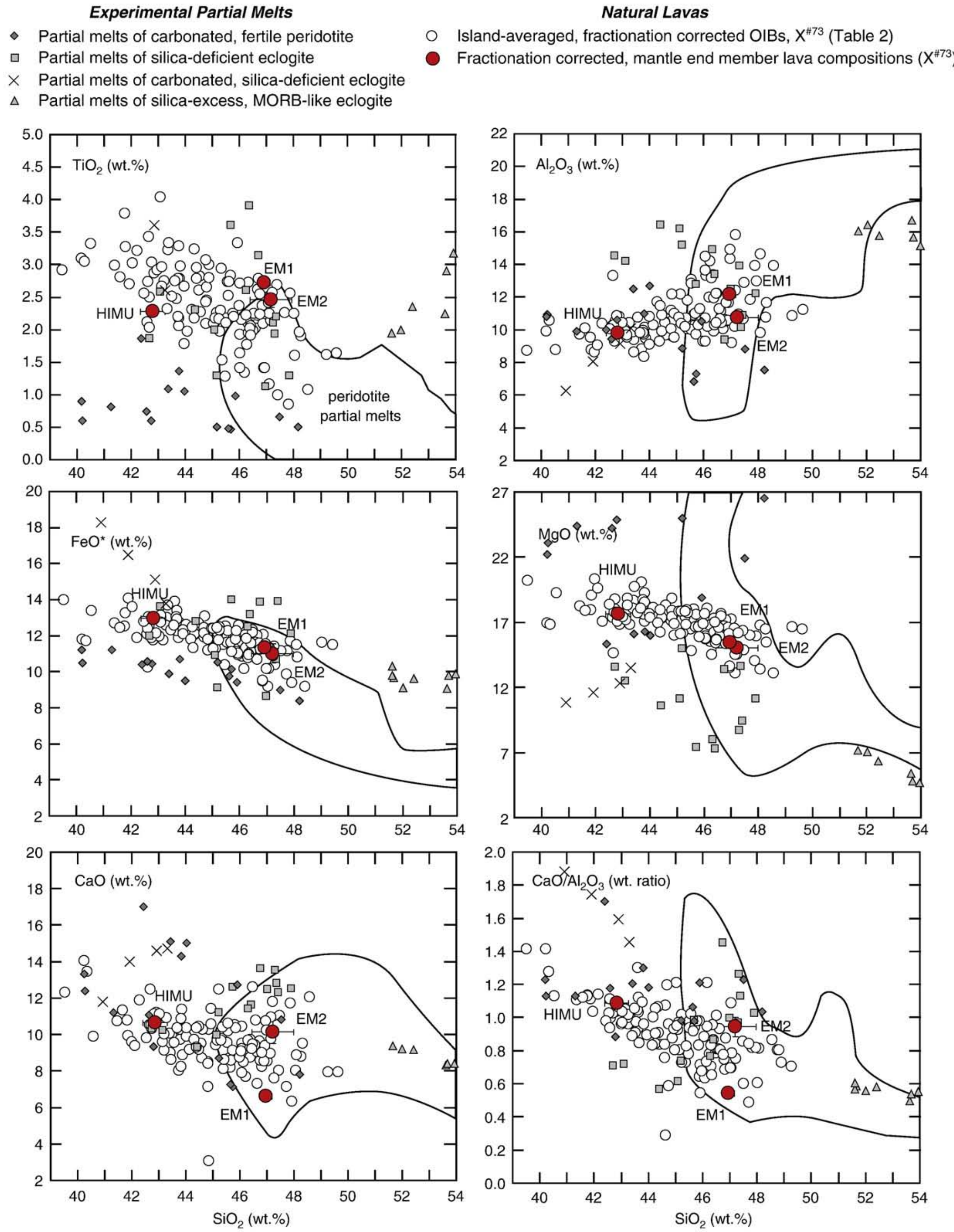

Fig. 7. Comparison of island-averaged, fractionation corrected OIBs (compositions in equilibrium with Fo_{90}, corrected by olivine addition; Table 2) with experimental partial melts. Also shown for reference are the primary magma estimates of HIMU, EM1, and EM2 mantle end members from Jackson and Dasgupta (2008). The fields of peridotite partial melts are based on experiments for pressures up to 7 GPa, from studies mentioned in the caption of Fig. 6. Partial melts of volatile-free, MORB-like eclogite are from 2.5 to 5.0 GPa (Yaxley and Green, 1998; Pertermann and Hirschmann, 2003; Spandler et al., 2008), for silica-deficient pyroxenite/eclogite from 2.0 to 5.0 GPa (Kogiso et al., 2003; Hirschmann et al., 2003; Kogiso and Hirschmann, 2006), for carbonated, silica-deficient eclogite from 3.0 GPa (Dasgupta et al., 2006), and for carbonated fertile peridotite from 3 GPa (Hirose, 1997; Dasgupta et al., 2007).

FeO*–SiO_2 trend (hereafter referred as Fe–Si trend) of oceanic basalts. In Fig. 6, we plot the fractionation corrected FeO* and SiO_2 concentrations of island-averaged, primary OIBs from Table 2 and Supplementary Table 2 and compare them with basalts from oceanic spreading centers and laboratory experiments on mantle peridotite from a range of pressures.

The Fe–Si trend in oceanic basalts is conventionally taken to reflect the depth of melting or melt–mantle equilibration, with deeper melt extraction giving rise to higher FeO* and lower SiO_2 (Langmuir et al., 1992). Indeed, our compilation of island averaged basalts does present a negative trend in Fe–Si space (Fig. 6). However, excluding the islands that are located at or near mid-ocean ridges (Iceland, Azores, Galapagos, Jan Mayen, Amsterdam-Saint Paul, and Easter), the Fe–Si trend given by the intra-plate OIBs has a distinctly gentler slope (−0.21) compared to the Fe–Si trend observed in experimental partial melts of volatile-free peridotite (Fig. 6). The Fe–Si trend given by experimental partial melts of volatile-free peridotite from low to high pressure (slope of ~−1 for volatile-free peridotite partial melts generated between 2.5 and 7 GPa) overlaps the field of MORB and ridge-influenced ocean islands but does not cover the major element extrema of intraplate OIBs. The observed slope of intra-plate OIB Fe–Si trend does not change if OIB data are plotted without any fractionation correction, i.e., with MgO in the range of 10–16 wt.% (Fig. 6A). The trend also remains similar if island averaged OIBs are corrected to different primary Mg#s in the range 65 to 77 (equilibrium olivine of Fo_{86} to Fo_{92}) (Fig. 6B). Hence the obliquity between the Fe–Si trend defined by volatile-free peridotite partial melts and that defined by the natural OIB data is not eliminated simply by changing the Mg# of source peridotite. The intraplate OIBs' Fe–Si trend is anchored by at least two additional components that are off the peridotite partial melts trend: one that is richer in SiO_2 with moderately high FeO* (found only at Hawaii) at a given SiO_2 and the other that is poorer in SiO_2 and with high FeO* (found predominantly in lavas with a HIMU signature).

4.4. Plausible source lithologies that can contribute to the major element extrema of global OIBs

We have demonstrated that volatile-free peridotite alone cannot produce the major element compositional extrema of OIBs globally. Although the high MgO content and high Mg# of most primitive primary magmas (Supplementary Table 1) suggest involvement of mantle peridotite, generation of magmas solely from volatile-free peridotite with <45 wt.% SiO_2 remains a challenge. This is critical not only because most ocean islands erupt strongly silica undersaturated, alkalic magmas (Supplementary Table 1; Table 2), but also because the HIMU mantle end member produces such a magma composition (Jackson and Dasgupta, 2008). We observe that the major element extrema of global OIBs are most well sampled in islands on thick lithospheres. This suggests that the mantle lithologies that contribute to such magmas likely have deeper solidi compared to fertile peridotite and hence contribute preferentially to islands where average depths of decompression melting are restricted to greater depths, i.e., deeper LABs.

Attempts have been made to explore melting behavior of plausible, more easily fusible lithologies that generate major element compositional features such as high and low SiO_2 magmas with high FeO*. For generating silica-deficient and FeO*-rich, HIMU-type magmas the two candidates that appear most appealing are silica-deficient pyroxenite/eclogite (Kogiso et al., 2003; Hirschmann et al., 2003; Keshav et al., 2004; Kogiso and Hirschmann, 2006) or carbonated peridotite (Hirose, 1997; Dasgupta et al., 2007). Silica-deficient pyroxenites generate many of the features of low-SiO_2, high-FeO* end member magma (Fig. 7) similar to those produced by mantle end member HIMU (Jackson and Dasgupta, 2008). However, the partial melts of these lithologies are too rich in Al_2O_3 and too poor in TiO_2 to be contributing to HIMU-like partial melts (Fig. 7). Moreover, subduction, which is likely the most dominant process of creating eclogitic heterogeneity in the mantle, is unlikely to supply silica-deficient eclogite/garnet pyroxenite lithologies to the OIB source regions. Partial melting of carbonated peridotite can generate sufficiently silica-poor magmas, but experimental partial melts of natural carbonated peridotite are poorer in FeO* and TiO_2 as compared to primary OIBs (Hirose, 1997; Dasgupta et al., 2007). Perhaps the best candidate to supply the necessary enrichment to peridotite partial melt is silicate partial melts of carbonated eclogite. Experimental constraints on partial melts of carbonated eclogite, to date, remain limited (Dasgupta et al., 2006), but partial melts of silica-deficient, ilmenite bearing, carbonated eclogite does produce extreme enrichment of TiO_2, FeO*, and pronounced depletion in Al_2O_3 at sufficiently low SiO_2 contents (Dasgupta et al., 2006). Further experiments on carbonated eclogite, especially on carbonated MORB-like or silica-excess eclogite, will be necessary to test whether a more common variety of eclogite when fluxed by carbonate or CO_2 can generate a silica-deficient magma component required for many primary OIBs.

For the silica-rich component, i.e., tholeiitic magmas approaching or exceeding 50 wt.% SiO_2, MORB-like silica-excess eclogite is likely the most viable candidate. High pressure partial melting of this lithology, at high extent of melting, produces basaltic liquid with >52 wt.% silica and 8–10 wt.% FeO* (Fig. 7; Yaxley and Green, 1998; Pertermann and Hirschmann, 2003; Spandler et al., 2008).

Although we prefer carbonated eclogite and silica-excess (CO_2-free), MORB-like eclogite as the two end-member sources in addition to mantle peridotite, their physical presence may only be restricted to the deeper part of OIB source regions, owing to deeper solidi. The exact petrologic process of melt contributions from these fertile lithologies likely involves formation of secondary lithologies at shallower, more proximal mantle source regions. The secondary lithologies, if present at shallow depths, may form either by solid-state reaction of peridotite and eclogite or by eclogite melt (±CO_2)-peridotite reaction. The latter possibility is similar to the model put forward by Sobolev et al. (2005, 2007). Although it is not clear at this point, owing to lack of experimental data, the exact nature of plausible reactions between mantle peridotite and end member heterogeneities (silica–excess eclogite and carbonated eclogite and partial melts derived from them), but in any case, these reactive processes are likely important to explain relatively high-MgO, high-Ni compositions of many OIBs.

5. Concluding remarks

Our study demonstrates that global scale major element array of near-primary OIBs cannot be generated from a volatile-free, homogeneous peridotite source by variation in melting conditions. Islands occurring at or near mid-ocean ridges, i.e., with shallow LABs, preserve compositions that are influenced strongly by the depth of melting. In these islands, greater extent of peridotite melting at shallow depths dilutes the contributions from compositional heterogeneities and major element signals from mantle lithological heterogeneities are subtle. But compositional variations for islands on intermediate to thick lithospheres (LAB at the time of volcanism ≥70 km) clearly require variation in source compositions. Variation in the mean depth of melting of volatile-free peridotite, owing either to a variation in mantle potential temperature or to lithospheric thickness, cannot produce the major element compositional extrema that anchor the global trends in compositional spaces such as $SiO_2^{\#73}$–$FeO^{*\#73}$, $SiO_2^{\#73}$–$[CaO/Al_2O_3]^{\#73}$, $SiO_2^{\#73}$–$TiO_2^{\#73}$. Basalts erupted on thicker lithospheres preserve the compositional extrema, including lavas with low SiO_2 and high FeO* (HIMU-like component), and lavas with high SiO_2 and moderately high FeO* (Hawaiian Koolau-like component). These components are well preserved for islands on thicker lithospheres presumably because deeper LABs prevent significant shallower melting of peridotite and preferentially collect contributions from more fertile sources that have deeper solidi.

Comparison of experimental partial melts with primary OIBs in SiO_2–FeO* space indicate that two additional higher Fe components – one richer in SiO_2 and the other poorer in SiO_2 – need to be present in the mantle peridotite source to explain the OIB chemistry globally. Comparison of experimental partial melts of all the plausible mantle lithologies with the target major element compositions of primary OIBs suggests that silica-excess eclogite and carbonated eclogite are the two most viable candidates. These enriched components are not sampled everywhere and their distribution suggests a heterogeneous distribution of major element and volatile heterogeneities in the mantle.

Acknowledgements

This work benefited from supportive and thoughtful formal reviews by Alex Sobolev and Tim Elliott. The authors also acknowledge informal critique by Claude Herzberg. This work received support from NSF grant EAR-0911442 and Rice University start-up grant to RD. MGJ was supported by a postdoctoral fellowship from the Carnegie Institution of Washington.

Appendix A. Supplementary data

Supplementary data associated with this article can be found, in the online version, at doi:10.1016/j.epsl.2009.11.027.

References

Azevedo, J.M.M., Portugal Ferreira, M.R., 2006. The volcanotectonic evolution of Flores Island, Azores (Portugal). J. Volcanol. Geotherm. Res. 156, 90–102.
Baker, M.B., Hirschmann, M.M., Ghiorso, M.S., Stolper, E.M., 1995. Compositions of near-solidus peridotite melts from experiments and thermodynamic calculations. Nature 375, 308–311. doi:10.1038/375308a375300.
Binard, N., Maury, R.C., Guille, G., Talandier, J., Gillot, P.Y., Cotten, J., 1993. Mehetia Island, South Pacific: geology and petrology of the emerged part of the Society hot spot. J. Volcanol. Geotherm. Res. 55, 239–260.
Bock, G.n., 1991. Long-period S to P converted waves and the onset of partial melting beneath Oahu, Hawaii. Geophys. Res. Lett. 18, 869–872.
Bonhommet, N., Beeson, M.H., Dalrymple, G.B., 1977. A contribution to the geochronology and petrology of the island of Lanai, Hawaii. Geol. Soc. Amer. Bull. 88, 1282–1286.
Bulatov, V.K., Girnis, A.V., Brey, G.P., 2002. Experimental melting of a modally heterogeneous mantle. Mineral. Petrol. 75, 131–152.
Burke, K., 2001. Origin of the Cameroon line of Volcano-capped swells. J. Geol. 109, 349–362.
Calvert, A.T., Moore, R.B., McGeehin, J.P., Rodrigues da Silva, A.M., 2006. Volcanic history and $^{40}Ar/^{39}Ar$ and ^{14}C geochronology of Terceira Island, Azores, Portugal. J. Volcanol. Geotherm. Res. 156, 103–115.
Camps, P., Henry, B., Prévot, M., Faynot, L., 2001. Geomagnetic paleosecular variation recorded in Plio-Pleistocene volcanic rocks from Possession Island (Crozet Archipelago, southern Indian Ocean). J. Geophys. Res. 106, 1961–1971.
Caplan-Auerbach, J., Duennebier, F., Ito, G., 2000. Origin of intraplate volcanoes from guyot heights and oceanic paleodepth. J. Geophys. Res. 105, 2679–2697.
Caress, D.W., McNutt, M.K., Detrick, R.S., Mutter, J.C., 1995. Seismic imaging of hotspot-related crustal underplating beneath the Marquesas Islands. Nature 373, 600–603.
Carracedo, J.C., Day, S., Guillou, H., Rodriguez Badiola, E., Canas, J.A., Perez Torrado, F.J., 1998. Hotspot volcanism close to a passive continental margin; the Canary Islands. Geol. Mag. 135, 591–604.
Carracedo, J.C., Pérez Torrado, F.J., Ancochea, E., Meco, J., Hernán, F., Cubas, C.R., Casillas, R., Rodríguez Badiola, E., Ahijado, A., 2002. Cenozoic volcanism II: the Canary Islands. In: Gibbons, W., Moreno, T. (Eds.), The Geology of Spain, vol. 18. The Geological Society London, London, pp. 439–472.
Chaffey, D.J., Clif, R.A., Wilson, B.M., 1989. Characterization of the St Helena magma source. In: Saunders, A.D., Norry, M.J. (Eds.), Magmatism in the Ocean Basins, vol. 42. Geological Society of London, London, pp. 257–276.
Chauvel, C., McDonough, W., Guille, G., Maury, R., Duncan, R., 1997. Contrasting old and young volcanism in Rurutu Island, Austral chain. Chem. Geol. 139, 125–143.
Clément, J.-P., Legendre, C., Caroff, M., Guillou, H., Cotten, J., Bollinger, C., Guille, G., 2003. Epiclastic deposits and 'horseshoe-shaped' calderas in Tahiti (Society Islands) and Ua Huka (Marquesas Archipelago), French Polynesia. J. Volcanol. Geotherm. Res. 120, 87–101.
Clouard, V., Bonneville, A., 2004. Submarine landslides in Society and Austral Islands, French Polynesia: evolution with the age of edifices. In: Hekinian, R. (Ed.), Submarine landslides in French Polynesia, Oceanic Hotspots. Springer-Verlag, pp. 209–238.
Danobeitia, J.J., Canales, J.P., 2000. Magmatic underplating in the Canary Archipelago. J. Volcanol. Geotherm. Res. 103, 27–41.
Dasgupta, R., Hirschmann, M.M., Stalker, K., 2006. Immiscible transition from carbonate-rich to silicate-rich melts in the 3 GPa melting interval of eclogite + CO_2 and genesis of silica-undersaturated ocean island lavas. J. Petrol. 47, 647–671.
Dasgupta, R., Hirschmann, M.M., Smith, N.D., 2007. Partial melting experiments of peridotite + CO_2 at 3 GPa and genesis of alkalic ocean island basalts. J. Petrol. 48, 2093–2124.
Davis, F.A., Tangeman, J.A., Tenner, T.J., Hirschmann, M.M., 2009. The composition of KLB-1 peridotite. Am. Mineral. 94, 176–180.
Desonie, D.L., Duncan, R.A., Natland, J.H., 1993. Temporal and geochemical variability of volcanic products of the Marquesas hotspot. J. Geophys. Res. 98, 17,649–617,665.
Duncan, R.A., McDougall, I., 1976. Linear volcanism in French Polynesia. J. Volcanol. Geotherm. Res. 1, 197–227.
Duprat, H.I., Friis, J., Holm, P.M., Grandvuinet, T., Sørensen, R.V., 2007. The volcanic and geochemical development of São Nicolau, Cape Verde Islands: constraints from field and 40Ar/39Ar evidence. J. Volcanol. Geotherm. Res. 162, 1–19.
Dupuy, C., Vidal, P., Barsczus, H.G., Chauvel, C., 1987. Origin of basalts from the Marquesas Archipelago (south central Pacific Ocean): isotope and trace element constraints. Earth Planet. Sci. Lett. 82, 145–152.
Dupuy, C., Vidal, P., Maury, R., Guille, G., 1993. Basalts from Mururoa, Fangataufa and Gambier islands (French Polynesia): geochemical dependence on the age of the lithosphere. Earth Planet. Sci. Lett. 117, 89–100.
Ellam, R.M., 1992. Lithospheric thickness as a control on basalt geochemistry. Geology 20, 153–156.
Elliott, T., Blichert-Toft, J., Heumann, A., Koetsier, G., Forjaz, V., 2007. The origin of enriched mantle beneath São Miguel, Azores. Geochim. Cosmochim. Acta 71, 219–240.
Falloon, T.J., Green, D.H., Danyushevski, L.V., Faul, U.H., 1999. Peridotite melting at 1 0 and 1 5 GPa: an experimental evaluation of techniques using diamond aggregates and mineral mixes for determination of near-solidus melts. J. Petrol. 40, 1343–1375.
Falloon, T.J., Danyushevsky, L.V., Green, D.H., 2001. Peridotite melting at 1 GPa: reversal experiments on partial melt composition produced by peridotite-basalt sandwich experiments. J. Petrol. 42, 2363–2390.
Farley, K.A., Basu, A.R., Craig, H., 1993. He, Sr and Nd isotopic variations in lavas from the juan fernandez archipelago, SE pacific. Contrib. Mineral. Petrol. 115, 75–87.
Feraud, G., Kaneoka, I., Allègre, C.J., 1980. K/Ar ages and stress pattern in the Azores: geodynamic implications. Earth Planet. Sci. Lett. 46, 275–286.
Féraud, G., Schmincke, H.-U., Lietz, J., Gastaud, J., Pritchard, G., Bleil, U., 1981. New K–Ar ages, chemical analyses and magnetic data of rocks from the sland of Santa Maria (Azores), Porto Santo and Madeira (Madeira Archipelago) and Gran Canaria (Canary Islands). Bull. Volcanol. 44, 359–375.
Gaffney, A.M., Nelson, B.K., Blichert-Toft, J., 2005. Melting in the Hawaiian plume at 1–2 Ma as recorded at Maui Nui: the role of eclogite, peridotite, and source mixing. Geochem. Geophys. Geosyst. 6, Q10L11. doi:10.1029/2005GC000927.
Gass, I.G., 1967. Geochronology of the Tristan da Cunha group of islands. Geol. Mag. 104, 160–170.
Gast, P.W., Tilton, G.R., Hedge, C., 1964. Isotopic composition of lead and strontium from ascension and Gough Islands. Science 145, 1181–1185.
Geldmacher, J., van den Bogaard, P., Hoernle, K., Schmincke, H.-U., 2000. The $^{40}Ar/^{39}Ar$ age dating of the Madeira archipelago and hotspot track (eastern North Atlantic). Geochem. Geophys. Geosyst. 1, 1008. doi:10.1029/1999GC000018.
Geldmacher, J., Hoernle, K., van den Bogaard, P., Zankl, G., Garbe-Schönberg, D., 2001. Earlier history of the ≥70 Ma-old Canary hotspot based on the temporal and geochemical evolution of the Selvagen Archipelago and neighboring seamounts in the Eastern North Atlantic. J. Volcanol. Geotherm. Res. 111, 55–87.
Geldmacher, J., Hoernle, K., Bogaard, P.v.d., Duggen, S., Werner, R., 2005. New $^{40}Ar/^{39}Ar$ age and geochemical data from seamounts in the Canary and Madeira volcanic provinces: Support for the mantle plume hypothesis. Earth Planet. Sci. Lett. 237, 85–101.
Gerlach, D.C., Stormer Jr., J.C., Mueller, P.A., 1987. Isotopic geochemistry of Fernando de Noronha. Earth Planet. Sci. Lett. 85, 129–144.
Gillot, P.Y., Nativel, P., 1982. K–Ar chronology of the ultimate activity of piton des neiges volcano, reunion island, Indian ocean. J. Volcanol. Geotherm. Res. 13, 131–146.
Gillot, P.Y., Nativel, P., 1989. Eruptive history of the Piton de la Fournaise volcano, Reunion Island, Indian Ocean. J. Volcanol. Geotherm. Res. 36, 53–65.
Gripp, A.E., Gordon, R.G., 2002. Young tracks of hotspots and current plate velocities. Geophys. J. Int. 150, 321–361.
Grove, T.L., Juster, T.C., 1989. Experimental investigations of low-Ca pyroxene stability and olivine-pyroxene-liquid equilibria at 1-atm in natural basaltic and andesitic liquids. Contrib. Mineral. Petrol. 103, 287–305.
Guillou, H., Garcia, M.O., Turpin, L., 1997. Unspiked K–Ar dating of young volcanic rocks from Loihi and Pitcairn hot spot seamounts. J. Volcanol. Geotherm. Res. 78, 239–249.
Haase, K.M., 1996. The relationship between the age of the lithosphere and the composition of oceanic magmas: constraints on partial melting, mantle sources and the thermal structure of the plates. Earth Planet. Sci. Lett. 144, 75–92.
Haase, K.M., Stoffers, P., Garbe-Schonberg, C.D., 1997. The petrogenetic evolution of lavas from Easter Island and neighbouring seamounts, near-ridge hotspot volcanoes in the SE Pacific. J. Petrol. 38, 785–813.
Hall, P.S., Kincaid, C., 2003. Melting, dehydration, and the dynamics of off-axis plume-ridge interaction. Geochem. Geophys. Geosyst. 4, 8510. doi:10.1029/2003gc000567.
Hart, S.R., 1971. K, Rb, Cs, Sr and Ba contents and Sr isotope ratios of ocean floor basalts. Philos. Trans. R. Soc. Lond. 268, 573–587.
Hauri, E.H., 1996. Major-element variability in the Hawaiian mantle plume. Nature 382, 415–419.
Herrero-Bervera, E., Margas-Viñuela, J., Valet, J.P., 2000. Paleomagnetic study of the ages of lavas on the island of Lanai'i, Hawai'i. J. Volcanol. Geotherm. Res. 104, 21–31.
Herzberg, C., Asimow, P.D., 2008. Petrology of some oceanic island basalts: PRIMELT2.XLS software for primary magma calculation. Geochem. Geophys. Geosyst 9, Q09001. doi:10.1029/02008GC002057.
Herzberg, C., Gazel, E., 2009. Petrological evidence for secular cooling in mantle plumes. Nature 458, 619–622.

Herzberg, C., Gasparik, T., Sawamoto, H., 1990. Origin of mantle peridotite: constraints from melting experiments to 16.5 GPa. J. Geophys. Res. 95, 15,779–715,803. doi:10.1029/JB1095iB1010p15779.
Hirose, K., 1997. Partial melt compositions of carbonated peridotite at 3 GPa and role of CO_2 in alkali-basalt magma generation. Geophys. Res. Lett. 24, 2837–2840.
Hirose, K., Kushiro, I., 1993. Partial melting of dry peridotites at high pressures: determination of compositions of melts segregated from peridotite using aggregates of diamond. Earth Planet. Sci. Lett. 114, 477–489.
Hirschmann, M.M., Kogiso, T., Baker, M.B., Stolper, E.M., 2003. Alkalic magmas generated by partial melting of garnet pyroxenite. Geology 31, 481-484.
Hofmann, A.W., 1997. Mantle geochemistry: the message from oceanic volcanism. Nature 385, 219–229.
Hofmann, A.W., White, W.M., 1982. Mantle plumes from ancient oceanic crust. Earth Planet. Sci. Lett. 57, 421–436.
Holm, P.M., Wilson, J.R., Christensen, B.P., Hansen, L., Hansen, S.L., Hein, K.M., Mortensen, A.K., Pedersen, R., Plesner, S., Runge, M.K., 2006. Sampling the Cape Verde Mantle Plume: Evolution of Melt Compositions on Santo Antão, Cape Verde Islands. J. Petrol. 47, 145–189.
Huang, S., Frey, F.A., 2005. Recycled oceanic crust in the Hawaiian Plume: evidence from temporal geochemical variations within the Koolau Shield. Contrib. Mineral. Petrol. 149, 556–575.
Humphreys, E.R., Niu, Y., 2009. On the composition of ocean island basalts (OIB): the effects of lithospheric thickness variation and mantle metasomatism. Lithos 112, 118–136.
Imsland, P., 1986. The volcanic eruption on Jan Mayen, January 1985: interaction between a volcanic island and a fracture zone. J. Volcanol. Geotherm. Res. 28, 45–53.
Jackson, M.G., Dasgupta, R., 2008. Compositions of HIMU, EM1, and EM2 from global trends between radiogenic isotopes and major elements in ocean island basalts. Earth Planet. Sci. Lett. 276, 175–186. doi:10.1016/j.epsl.2008.1009.1023.
Jackson, M.G., Hart, S.R., Koppers, A.A.P., Staudigel, H., Konter, J., Blusztajn, J., Kurz, M., Russell, J.A., 2007. The return of subducted continental crust in Samoan lavas. Nature 448, 684–687.
Jancin, M., Young, K.D., Voight, B., Aronson, J.L., Saemundsson, K.n., 1985. Stratigraphy and K/Ar ages across the west flank of the northeast Iceland axial rift zone, in relation to the 7 Ma-tectonic reorganization of Iceland. J. Geophys. Res. 90, 9961–9985.
Johnson, K.T.M., Graham, D.W., Rubin, K.H., Nicolaysen, K., Scheirer, D.S., Forsyth, D.W., Baker, E.T., Douglas-Priebe, L.M., 2000. Boomerang Seamount: the active expression of the Amsterdam-St. Paul hotspot, Southeast Indian Ridge. Earth Planet. Sci. Lett. 183, 245–259.
Keating, B.H., Mattey, D.P., Helsley, C.E., Naughton, J.J., Epp, D., Lazarewicz, A., Schwank, D., 1984. Evidence for a hot spot origin of the Caroline Islands. J. Geophys. Res. 89, 9937–9948.
Keshav, S., Gudfinnsson, G.H., Sen, G., Fei, Y., 2004. High-pressure melting experiments on garnet clinopyroxenite and the alkalic to tholeiitic transition in ocean-island basalts. Earth Planet. Sci. Lett. 223, 365–379.
Kinzler, R.J., 1997. Melting of mantle peridotite at pressures approaching the spinel to garnet transition: application to mid-ocean ridge basalt petrogenesis. J. Geophys. Res. 102, 853–874.
Kinzler, R.J., Grove, T.L., 1992. Primary magmas of mid-ocean ridge basalts 1. Experiments and methods. J. Geophys. Res. 97, 6885–6906.
Klein, E.M., Langmuir, C.H., 1987. Global correlations of ocean ridge basalt chemistry with axial depth and crustal thickness. J. Geophys. Res. 92, 8089–8115. doi:10.1029/JB8092iB8008p08089.
Kogiso, T., Hirschmann, M.M., 2006. Partial melting experiments of bimineralic eclogite and the role of recycled mafic oceanic crust in the genesis of ocean island basalts. Earth Planet. Sci. Lett. 249, 188–199.
Kogiso, T., Tatsumi, Y., Shimoda, G., Barsczus, G., 1997. High μ (HIMU) ocean island basalts in southern Polynesia: new evidence for whole mantle scale recycling of subducted oceanic crust. J. Geophys. Res. 102, 8085–8103.
Kogiso, T., Hirschmann, M.M., Frost, D.J., 2003. High-pressure partial melting of garnet pyroxenite: possible mafic lithologies in the source of ocean island basalts. Earth Planet. Sci. Lett. 216, 603–617.
Koppers, A.A.P., Russell, J.A., Jackson, M.G., Konter, J., Staudigel, H., Hart, S.R., 2008. Samoa reinstated as a primary hotspot trail. Geology 36, 435–438.
Kumar, P., Kind, R., Hanka, W., Wylegalla, K., Reigber, C., Yuan, X., Woelbern, I., Schwintzer, P., Fleming, K., Dahl-Jensen, T., Larsen, T.B., Schweitzer, J., Priestley, K., Gudmundsson, O., Wolf, D., 2005. The lithosphere–asthenosphere boundary in the North-West Atlantic region. Earth Planet. Sci. Lett. 236, 249–257.
Kurz, M.D., Geist, D., 1999. Dynamics of the Galapagos hotspot from helium isotope geochemistry. Geochim. Cosmochim. Acta 63, 4139–4156.
Kushiro, I., 1996. Partial melting of a fertile mantle peridotite at high pressures: an experimental study using aggregates of diamond. In: Basu, A., Hart, S. (Eds.), Earth Processes: Reading the Isotopic Code. American Geophysical Union, Washington, DC, pp. 109–122.
Landes, M., Ritter, J.R.R., Readman, P.W., 2007. Proto-Iceland plume caused thinning of Irish lithosphere. Earth Planet. Sci. Lett. 255, 32–40.
Langmuir, C.H., Klein, E.M., Plank, T., 1992. In: Phipps Morgan, J., Blackman, D.K., Sinton, J.M. (Eds.), Petrological systematics of mid-ocean ridge basalts: constraints on melt generation beneath ocean ridges. : Mantle flow and melt generation at mid-ocean ridges, vol. 71. American Geophysical Union, Washington, DC, pp. 183–280.
Lanyon, R., Varne, R., Crawford, A.J., 1993. Tasmanian tertiary basalts, the balleny plume, and opening of the tasman sea (southwest Pacific Ocean). Geology 21, 555–558.
Laporte, D., Toplis, M.J., Seyler, M., Devidal, J.-L., 2004. A new experimental technique for extracting liquids from peridotite at very low degrees of melting: application to partial melting of depleted peridotite. Contrib. Mineral. Petrol. 146, 463–484.
Lassiter, J.C., Blichert-Toft, J., Hauri, E.H., Barsczus, H.G., 2003. Isotope and trace element variations in lavas from Raivavae and Rapa, Cook-Austral islands: constraints on the nature of HIMU- and EM-mantle and the origin of mid-plate volcanism in French Polynesia. Chem. Geol. 202, 115–138.
Lee, C.-T.A., Luffi, P., Plank, T., Dalton, H., Leeman, W.P., 2009. Constraints on the depths and temperatures of basaltic magma generation on Earth and other terrestrial planets. Earth Planet. Sci. Lett. 279, 20–33.
Li, A., Detrick, R.S., 2006. Seismic structure of Iceland from Rayleigh wave inversions and geodynamic implications. Earth Planet. Sci. Lett. 241, 901–912.
Li, X., Kind, R., Priestley, K., Sobolev, S.V., Tilmann, F., Yuan, X., Weber, M., 2000. Mapping the Hawaiian plume conduit with converted seismic waves. Nature 405, 938–941.
Li, X., Kind, R., Yuan, X., Wölbern, I., Hanka, W., 2004. Rejuvenation of the lithosphere by the Hawaiian plume. Nature 427, 827–829.
Lodge, A., Helffrich, G., 2006. Depleted swell root beneath the Cape Verde Islands. Geology 34, 449–452.
Marzoli, A., Piccirillo, E.M., Renne, P.R., Bellieni, G., Iacumin, M., Nyobe, J.B., Tongwa, A.T., 2000. The Cameroon volcanic line revisited: petrogenesis of continental basaltic magmas from lithospheric and asthenospheric mantle sources. J. Petrol. 41, 87–109.
Maund, J.G., Rex, D.C., Le Roex, A.P., Reid, D.L., 1988. Volcanism on Gough Island: a revised stratigraphy. Geol. Mag. 125, 175–181.
McBirney, A.R., Gass, I.G., 1967. Relations of oceanic volcanic rocks to mid-oceanic rises and heat flow. Earth Planet. Sci. Lett. 2, 265–276.
McDougall, I.A.N., 1964. Potassium–argon ages from lavas of the Hawaiian Islands. Geol. Soc. Amer. Bull. 75, 107–128.
McDougall, I., 1979. Age of shield-building volcanism of Kauai and linear migration of volcanism in the Hawaiian island chain. Earth Planet. Sci. Lett. 46, 31–42.
McDougall, I.A.N., Verwoerd, W., Chevallier, L.U.C., 2001. K–Ar geochronology of Marion Island, Southern Ocean. Geol. Mag. 138, 1–17.
McKenzie, D., Jackson, J., Priestley, K., 2005. Thermal structure of oceanic and continental lithosphere. Earth Planet. Sci. Lett. 233, 337–349.
McNutt, M.K., Caress, D.W., Reynolds, J., Jordahl, K.A., Duncan, R.A., 1997. Failure of plume theory to explain midplate volcanism in the southern Austral islands. Nature 389, 479–482.
Mitchell, J.G., Le Bas, M.J., Zielonka, J., Furnes, H., 1983. On dating the magmatism of Maio, Cape Verde Islands. Earth Planet. Sci. Lett. 64, 61–76.
Moore, R.B., 1990. Volcanic geology and eruption frequency, Silo Miguel, Azores. Bull. Volcanol. 52, 602–614.
Mukhopadhyay, S., Lassiter, J.C., Farley, K.A., Bogue, S.W., 2003. Geochemistry of Kauai shield-stage lavas: implications for the chemical evolution of the Hawaiian plume. Geochem. Geophys. Geosyst. 4, 1009. doi:10.1029/2002GC000342.
Müller, R.D., Sdrolias, M., Gaina, C., Roest, W.R., 2008. Age, spreading rates, and spreading asymmetry of the world's ocean crust. Geochem. Geophys. Geosys. 9, Q04006. doi:10.1029/02007GC001743.
Naim, O., Cuet, P., Mangar, V., 2000. The Mascarene Islands. In: Mclanahan, T.R., Sheppard, C.R.C., Obura, D.O. (Eds.), Coral reefs of the Indian Ocean — Their ecology and conservation. Oxford University Press, New York, pp. 353–382.
Naughton, J.J., MacDonald, G.A., Greenberg, V.A., 1980. Some additional potassium–argon ages of Hawaiian rocks: the Maui volcanic complex of Molokai, Maui, Lanai and Kahoolawe. J. Volcanol. Geotherm. Res. 7, 339–355.
Neugebauer, H.J., 1987. Models of lithospheric thinning. Annual. Rev. Earth Planet. Sci. 15, 421–443.
Nicolaysen, K., Frey, F.A., Hodges, K.V., Weis, D., Giret, A., 2000. $^{40}Ar/^{39}Ar$ geochronology of flood basalts from the Kerguelen Archipelago, southern Indian Ocean: implications for Cenozoic eruption rates of the Kerguelen plume. Earth Planet. Sci. Lett. 174, 313–328.
Nisbet, E.G., Pearce, J.A., 1977. Clinopyroxene composition in mafic lavas from different tectonic settings. Contrib. Mineral. Petrol. 63, 149–160.
Nohda, S., Kaneoka, I., Hanyu, T., Xu, S., Uto, K., 2005. Systematic Variation of Sr-, Nd- and Pb-Isotopes with Time in Lavas of Mauritius, Reunion Hotspot. J. Petrol. 46, 505–522.
Nougier, J., Cantagrel, J.M., Carche, J.P., 1986. The Comores archipelago in the western Indian ocean: volcanology, geochronology and geodynamic setting. J. Afr. Earth. Sci. 5, 135–145.
O'Connor, J.M., Stoffers, P., Wijbrans, J.R., Worthington, T.J., 2007. Migration of widespread long-lived volcanism across the Galápagos Volcanic Province: evidence for a broad hotspot melting anomaly? Earth Planet. Sci. Lett. 263, 339–354.
O'Neill, C., Müller, D., Steinberger, B., 2003. Geodynamic implications of moving Indian Ocean hotspots. Earth Planet. Sci. Lett. 215, 151–168.
Pertermann, M., Hirschmann, M.M., 2003. Anhydrous partial melting experiments on MORB-like eclogite: Phase relations, phase compositions and mineral-melt partitioning of major elements at 2–3 GPa. J. Petrol. 44, 2173–2201.
Pickering-Witter, J., Johnston, A.D., 2000. The effects of variable bulk composition on melting systematics of fertile peridotitic assemblages. Contrib. Mineral. Petrol. 140, 190–211.
Plesner, S., Holm, P.M., Wilson, J.R., 2003. $^{40}Ar–^{39}Ar$ geochronology of Santo Antão, Cape Verde Islands. J. Volcanol. Geotherm. Res. 120, 103–121.
Priestley, K., Tilmann, F., 1999. Shear-wave structure of the lithosphere above the Hawaiian hot spot from two-station Rayleigh wave phase velocity measurements. Geophys. Res. Lett. 26, 1493–1496.
Prytulak, J., Elliot, T., 2007. TiO_2 enrichments in ocean island basalts. Earth Planet. Sci. Lett. 263, 388–403.
Recq, M., Goslin, J., Charvis, P., Operto, S., phane, 1998. Small-scale crustal variability within an intraplate structure: the Crozet Bank (southern Indian Ocean). Geophys. J. Int. 134, 145–156.
Robinson, J.A.C., Wood, B.J., Blundy, J.D., 1998. The beginning of melting of fertile and depleted peridotite. Earth Planet. Sci. Lett. 155, 97–111.

Sano, H., Sherrod, D.R., Tagami, T., 2006. Youngest volcanism about 1 million years ago at Kahoolawe Island, Hawaii. J. Volcanol. Geotherm. Res. 152, 91–96.
Schwab, B.E., Johnston, A.D., 2001. Melting systematics of modally variable, compositionally intermediate peridotites and the effects of mineral fertility. J. Petrol. 42, 1789–1811.
Schwarz, S., Klügel, A., van den Bogaard, P., Geldmacher, J., 2005. Internal structure and evolution of a volcanic rift system in the eastern North Atlantic: the Desertas rift zone, Madeira archipelago. J. Volcanol. Geotherm. Res. 141, 123–155.
Sobolev, A.V., Hofmann, A.W., Sobolev, S.V., Nikogosian, I.K., 2005. An olivine-free mantle source of Hawaiian shield basalts. Nature 434, 590–597.
Sobolev, A.V., Hofmann, A.W., Kuzmin, D.V., Yaxley, G.M., Arndt, N.T., Chung, S.-L., Danyushevsky, L.V., Elliot, T., Frey, F.A., Garcia, M.O., Gurenko, A.A., Kamenetsky, V.S., Kerr, A.C., Krivolutskaya, N.A., Matvienkov, V.V., Nikogosian, I.K., Rocholl, A., Sigurdsson, I.A., Sushchevskaya, N.M., Teklay, M., 2007. The amount of recycled crust in sources of mantle-derived melts. Science 316, 412–417.
Spandler, C., Yaxley, G., Green, D.H., Rosenthal, A., 2008. Phase relations and melting of anhydrous K-bearing eclogite from 1200 to 1600 C and 3 to 5 GPa. J Petrol. 49, 771–795. doi:10.1093/petrology/egm1039.
Standish, J., Geist, D., Harpp, K., Kurz, M.D., 1998. The emergence of a Galápagos shield volcano, Roca Redonda. Contrib. Mineral. Petrol. 133, 136–148.
Stein, C.A., Stein, S., 1992. A model for the global variation in oceanic depth and heat flow with lithospheric age. Nature 359, 123–129.
Swanson, F.J., Baitis, H.W., Lexa, J., Dymond, J., 1974. Geology of Santiago, Rabida, and Pinzon Islands, Galapagos. GSA Bull. 85, 1803–1810.
Takahashi, E., 1986. Melting of a dry peridotite KLB-1 up to 14 GPa: implications on the origin of peridotitic upper mantle. J. Geophys. Res. 91, 9367–9382.
Villagómez, D.R., Toomey, D.R., Hooft, E.E.E., Solomon, S.C., 2007. Upper mantle structure beneath the Galápagos Archipelago from surface wave tomography. J. Geophys. Res. 112, B07303. doi:10.1029/02006JB004672.
Villiger, S., Ulmer, P., Müntener, O., Thompson, A.B., 2004. The liquid line of descent of anhydrous, mantle-derived, tholeiitic liquids by fractional and equilibrium crystallization — an experimental study at 1.0 GPa. J. Petrol. 45, 2369–2388.
Walter, M.J., 1998. Melting of garnet peridotite and the origin of komatiite and depleted lithosphere. J. Petrol. 39, 29–60.
Wasylenki, L.E., Baker, M.E., Kent, A.R., Stolper, E.M., 2003. Near-solidus melting of the shallow upper mantle: partial melting experiments on depleted peridotite. J. Petrol. 44, 1163–1191.
Watts, A.B., ten Brink, U.S., Buhl, P., Brocher, T.M., 1985. A multichannel seismic study of lithospheric flexure across the Hawaiian-Emperor seamount chain. Nature 315, 105–111.
Weaver, B.L., 1991. The origin of ocean island basalt end-member compositions: trace element and isotopic constraints. Earth Planet. Sci. Lett. 104, 381–397.
Weis, D., Frey, F.A., Schlich, R., Schaming, M., Montigny, R., Damasceno, D., Mattielli, N., Nicolaysen, K.E., Scoates, J.S., 2002. Trace of the Kerguelen mantle plume: evidence from seamounts between the Kerguelen Archipelago and Heard Island, Indian Ocean. Geochem. Geophys. Geosyst. 3, 1033. doi:10.1029/2001gc000251.
White, W.M., McBirney, A.R., Duncan, R.A., 1993. Petrology and geochemistry of the Galápagos Islands: portrait of a pathological mantle plume. J. Geophys. Res. 98, 19533–19563.
Yaxley, G.M., Green, D.H., 1998. Reactions between eclogite and peridotite: mantle refertilisation by subduction of oceanic crust. Schweiz. Mineral. Petrogr. Mitt. 78, 243–255.
Zindler, A., Hart, S.R., 1986. Chemical geodynamics. Annual. Rev. Earth Planet. Sci. 14, 493–571.